

# ■ **WORK PORTFOLIO**

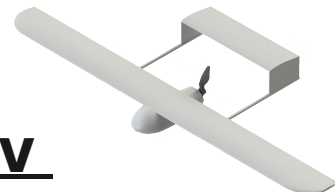
By : Shourya Sahdev



# Design Projects

01

Fixed Wing UAV



03

Quadcopter



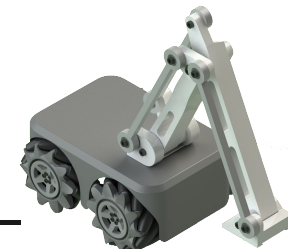
02

Recumbent Bicycle



04

Mobile Robotic Arm



# **Research Projects**

**05**

**Evaluating The Effect Of Process Parameters On Fsp Of  
Al5083 Alloy**

# **Coursework Projects**

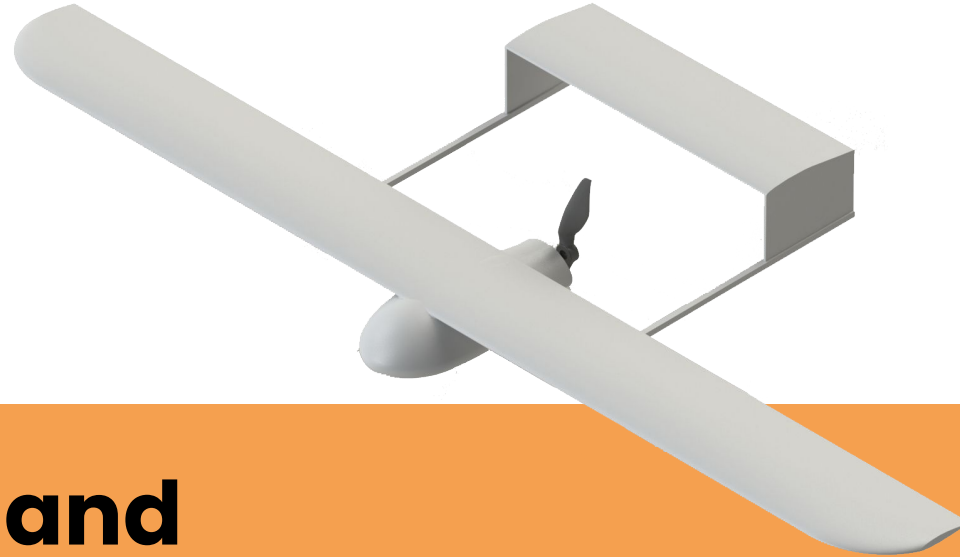
**06**

**Impact of Wing Sweep**

**07**

**Beam Impact Test**

# 01



## ■ Design and Optimization of a Fixed Wing UAV

# Step 1 – Iterative Weight Estimation

- Calculation of approximate weight using governing equations
- **Formula:**
  - Total Weight (kg) =  $W_{\text{Battery}} \text{ (kg)} + W_{\text{Propulsion}} \text{ (kg)} + W_{\text{Structural}} \text{ (kg)} + W_{\text{Payload}} \text{ (kg)}$
- **Historical data insights:**
  - Structural Weight: 15% - 40% of total weight
  - Propulsion System Weight: 5% - 20% of total weight
  - **Battery Weight Calculation:**
    - Energy Required (E.R.) = Power Required \* Time of Flight
    - Specific Energy Density (S.E.D.) = 100
    - Battery Weight = E.R. / S.E.D.
- **Values used:**
  - $W_{\text{Structural}} / \text{Total Weight} = 0.4$
  - $W_{\text{Propulsion}} / \text{Total Weight} = 0.15$
  - Velocity of UAV = 20 m/s
  - Time of flight = 1 hour
  - $W_{\text{Payload}} = 5 \text{ kg}$

# Weight Estimation Results

L/D	Total Weight (kg)	W_Battery (kg)	W_Propulsion (kg)	W_Structural (kg)
11	21.085466037687155	4.488459717014035	3.162819905653073	8.43418641507486
12	19.617897028617023	3.828053662924960	2.942684554292554	7.84715881144681
13	18.526795964657698	3.337058184148266	2.77901939469865	7.41071838586308
14	17.683770656183110	2.957696795327605	2.65256559842747	7.07350826247324
15	17.012852530687550	2.655783638861026	2.55192787960313	6.80514101227502
16	16.466218606081190	2.409798372788157	2.46993279091218	6.58648744243248

# Weight Estimation Results

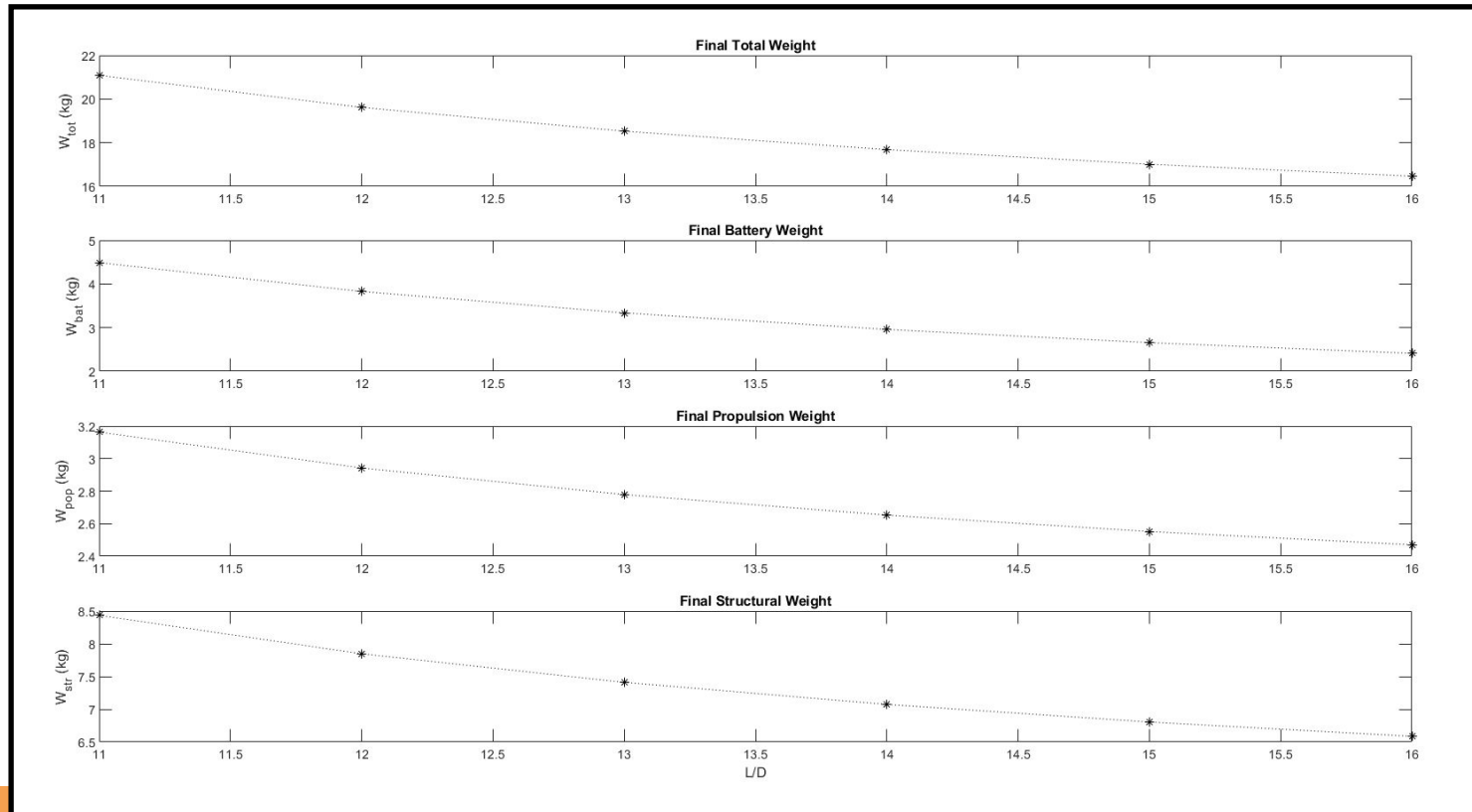


Figure: Weight components w.r.t.  $L/D$

## Step 2 – Estimation of Wing Geometric Parameters

- Calculation of following values using Weight for respective L/D values

- Formula:**

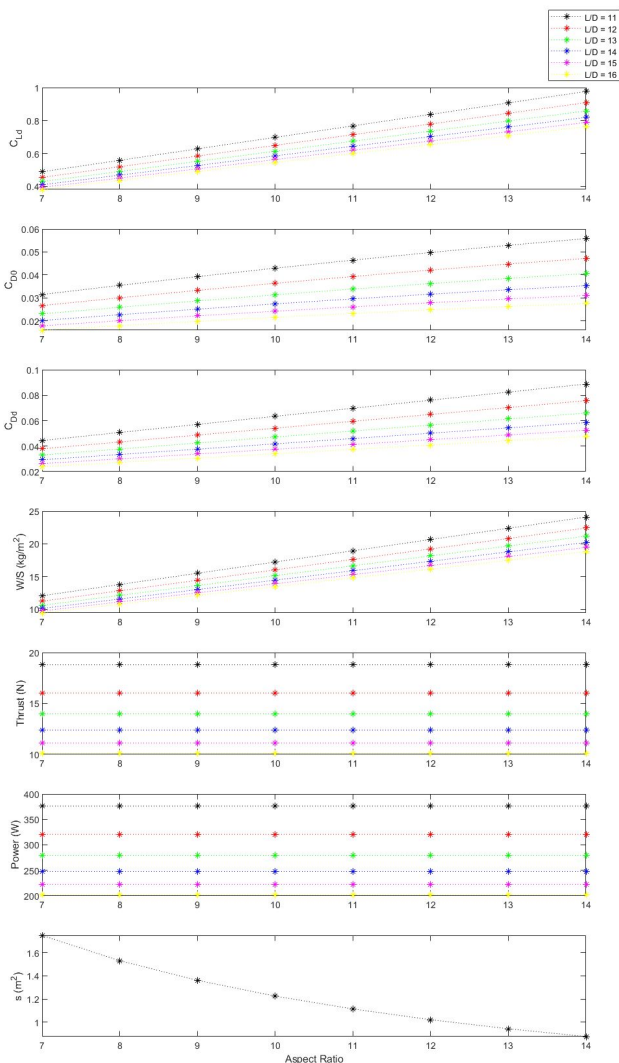
- Wing Area ( $S$ ) =  $b^2 / A.R.$
- Weight Ratio =  $W / S$
- $C_l = 2 * W / (S * V^2)$
- $C_Dd = C_l / (L/D)$
- $C_D0 = C_Dd - k * C_l^2$

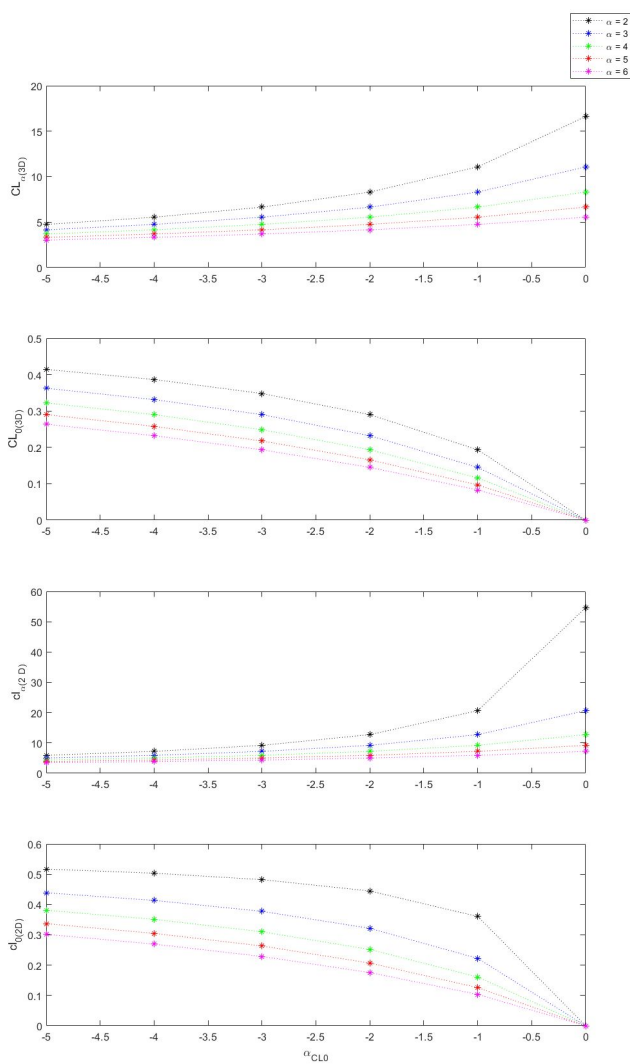
- Considerations:**

- High A.R. for aerodynamic efficiency
- Low A.R. for maneuverability

- Final target values:**

- |                                |                            |                          |
|--------------------------------|----------------------------|--------------------------|
| → $W/S = 14.45 \text{ kg/m}^2$ | → Thrust Required = 12.4 N | → $e = 0.76$             |
| → $C_D = 0.042$                | → Power Required = 250 W   | → $k = 0.042$            |
| → $C_D0 = 0.027$               | → Aspect Ratio = 10        | → $S = 1.23 \text{ m}^2$ |
| → $C_l = 0.58$                 | → Weight = 17.7 kg         | → $L/D = 14$             |





## Step 3: Airfoil Selection

- Calculation of  $CL_0(3D)$ ,  $CL(3D)$ ,  $Cl_0(2D)$ ,  $Cl(2D)$
- Formula:**
  - $CL\alpha(3D) = CL_d/\alpha_d - \alpha_{CL}=0$
  - $CL\alpha(3D) = Cl\alpha(2D) / [1 + (Cl\alpha(2D) / (\pi * e * A.R.))]$
  - $CL_0(3D) = CL$  of the airfoil for an infinite wing (at  $\alpha = 0$ )  
=  $CL\alpha(3D) * \alpha_{CL}=0$
  - $Cl_0(2D) = Cl\alpha(2D) / \alpha_{CL}=0$
- Iterating for  $Cl=0$  from -5 to 0 degrees and  $\alpha_d$  from 2 to 6 degrees following results were gathered using MATLAB (as shown in figure)
- Selected Airfoil: NACA 63-412
- Parameters:
  - $cL_0(2D) = 0.38$
  - $cL_{\alpha(2D)} = 7.21$
  - $CL_0(3D) = 0.29$
  - $CL_{\alpha(3D)} = 5.53$
  - $\alpha_d = 3$
  - $CL_d(3D) = 0.58$  (at  $\alpha_d = 3$ )
  - $\alpha_{CL}=0 = -3$

# Wing Geometry Design

- Design parameters:
  - Span(section 1) = 1.5 m
  - Span(section 2) = 0.25 m
  - Root chord = 0.37 m
  - Tip Chord = 0.37 m
  - Tip chord (section 2) = 0.2 m
  - Sweep (section 2) = 30 degrees
- The following characteristic curves were obtained for the wing geometry using OpenVSP

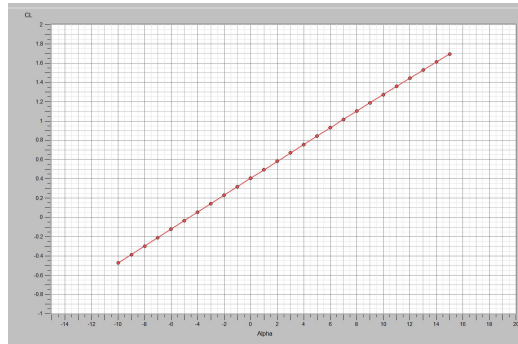


Figure:  $CL$  vs  $\alpha$

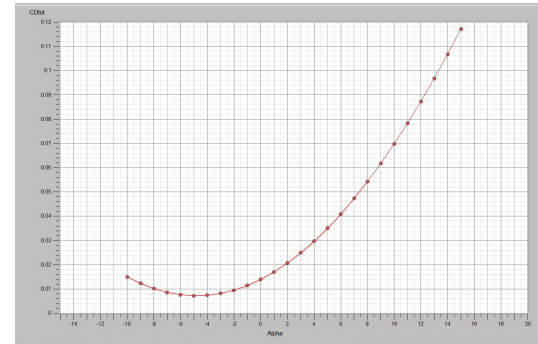


Figure:  $CD$  vs  $\alpha$

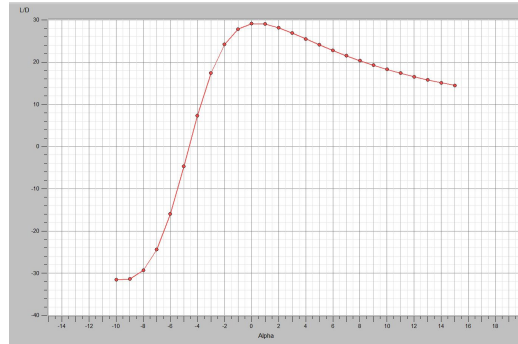


Figure:  $L/D$  vs  $\alpha$

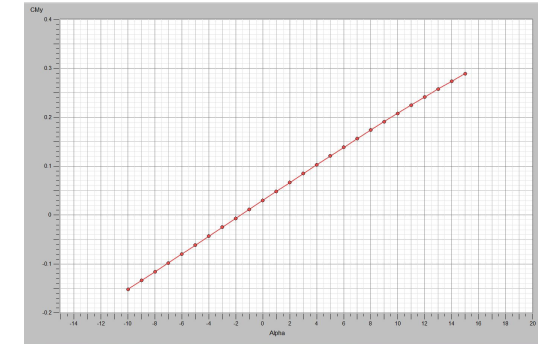


Figure:  $CM$  vs  $\alpha$

# Tail Geometry Design

- Selected Airfoil: NASA 64-012
- Parameters:
  - $b_T = 1.5 \text{ m}$
  - $ST = 0.35 \text{ m}$
- Calculated aerodynamic parameters:
  - $cL_{\alpha} \text{ (2D)} = 6.53$
  - $CL_{\alpha} \text{ (3D)} = 3.23$
- $X_{cg} = 0.18 \text{ m}$
- $X_{ac \text{ tail}} = 1.25 \text{ m}$

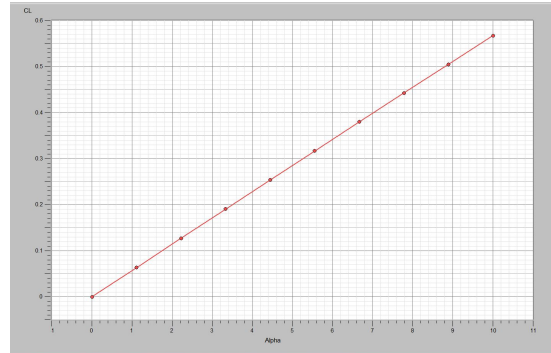


Figure:  $CL$  vs  $\alpha$

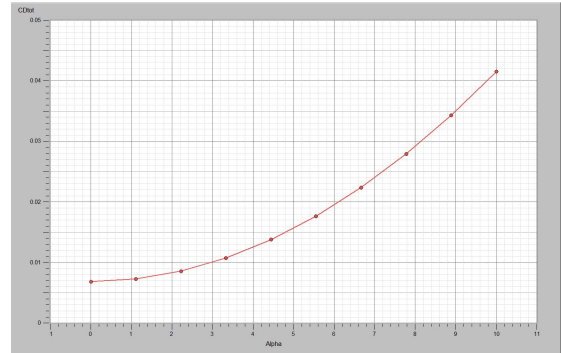


Figure:  $CD$  vs  $\alpha$

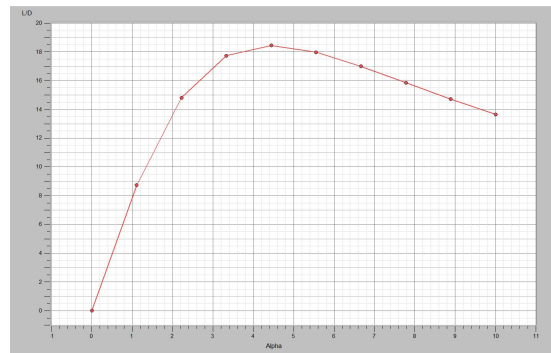


Figure:  $L/D$  vs  $\alpha$

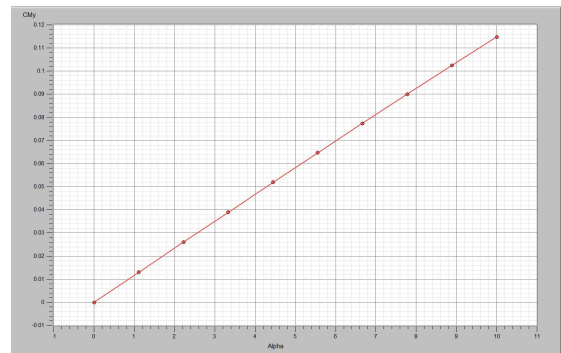


Figure:  $CM$  vs  $\alpha$

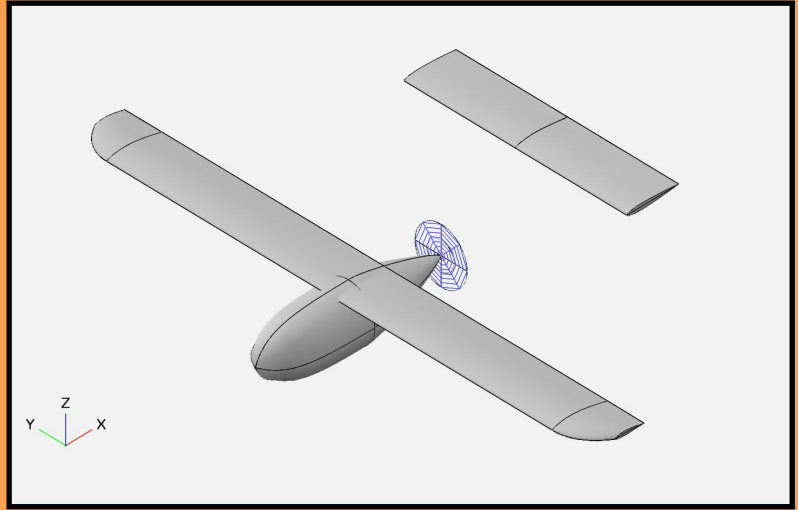


Figure: UAV Design in OpenVSP

# UAV Design Parameters

- Calculation of position of tail and center of gravity
- Key Formulas:
  - $Cm0 = Cmac\_wing + CL0_w * (x_{cg} - x_{ac\_wing})$
  - $Cm_{\alpha} = Cm_{\alpha}(wing) + CL_{\alpha}(wing) * (x_{cg} - x_{ac\_wing}) - (S_T/S) * CL_{\alpha}(tail) * (x_{ac\_tail} - x_{cg})$
  - $Cm0 + Cm_{\alpha} * \alpha_{trim} = 0$
- Values:
  - $x_{ac\_tail} = 1.25 \text{ m}$
  - $\alpha_{trim} = 3 \text{ degrees} = 0.051 \text{ radians}$
  - $x_{cg} = 0.18 \text{ m}$

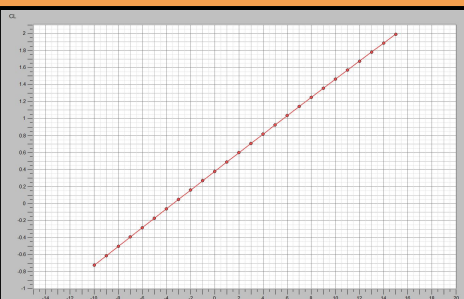


Figure: CL vs  $\alpha$

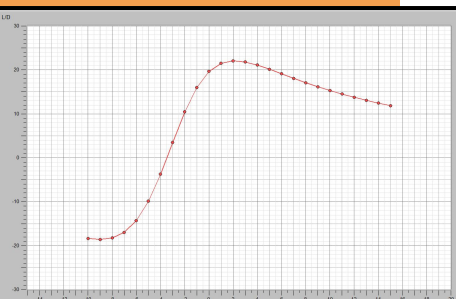


Figure: L/D vs  $\alpha$

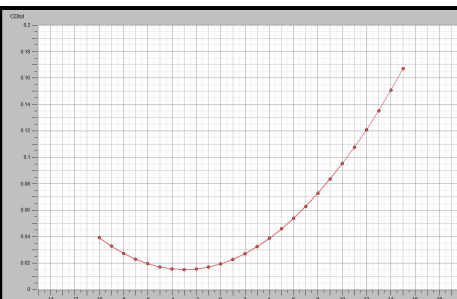


Figure: CD vs  $\alpha$

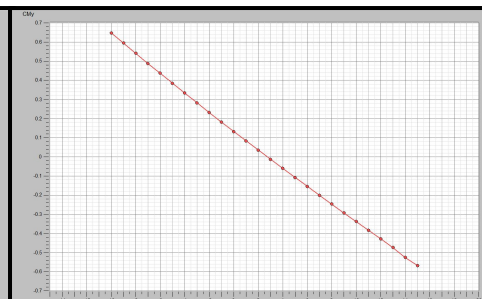


Figure: CM vs  $\alpha$

# UAV Design Parameters

Modeled the UAV design in SolidWorks and used CFD ANSYS to calculate the aerodynamic coefficients for the vehicle.

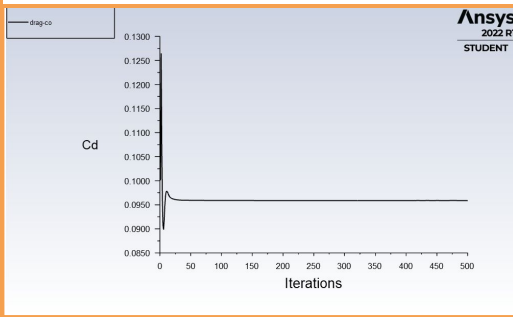


Figure: CD at  $\alpha = 0$

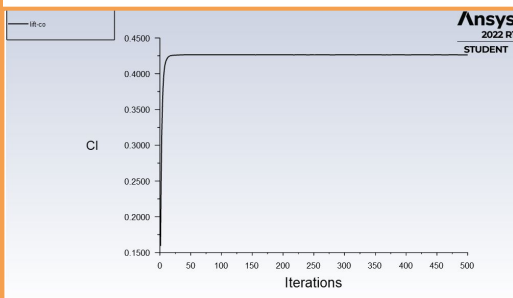


Figure: CD at  $\alpha = 0$

Zone	Forces [N]			Coefficients		
	Pressure	Viscous	Total	Pressure	Viscous	Total
uav	17.069147	5.5771561	22.646303	0.072274311	0.023614836	0.095889147
Net	17.069147	5.5771561	22.646303	0.072274311	0.023614836	0.095889147

$$\rightarrow CD(\alpha = 0) = 0.95$$

Zone	Forces [N]			Coefficients		
	Pressure	Viscous	Total	Pressure	Viscous	Total
uav	100.83605	-0.13727933	100.69877	0.42696077	-0.00058126918	0.4263795
Net	100.83605	-0.13727933	100.69877	0.42696077	-0.00058126918	0.4263795

$$\rightarrow CL(\alpha = 0) = 0.42$$

Zone	Forces [N]			Coefficients		
	Pressure	Viscous	Total	Pressure	Viscous	Total
uav	52.962975	6.2288942	59.191869	0.11212804	0.013187207	0.12531525
Net	52.962975	6.2288942	59.191869	0.11212804	0.013187207	0.12531525

$$\rightarrow CD(\alpha = 3) = 0.12$$

Zone	Forces [N]			Coefficients		
	Pressure	Viscous	Total	Pressure	Viscous	Total
uav	358.45996	-0.64495897	357.815	0.75889647	-0.0013654442	0.75753102
Net	358.45996	-0.64495897	357.815	0.75889647	-0.0013654442	0.75753102

$$\rightarrow CD(\alpha = 3) = 0.75$$

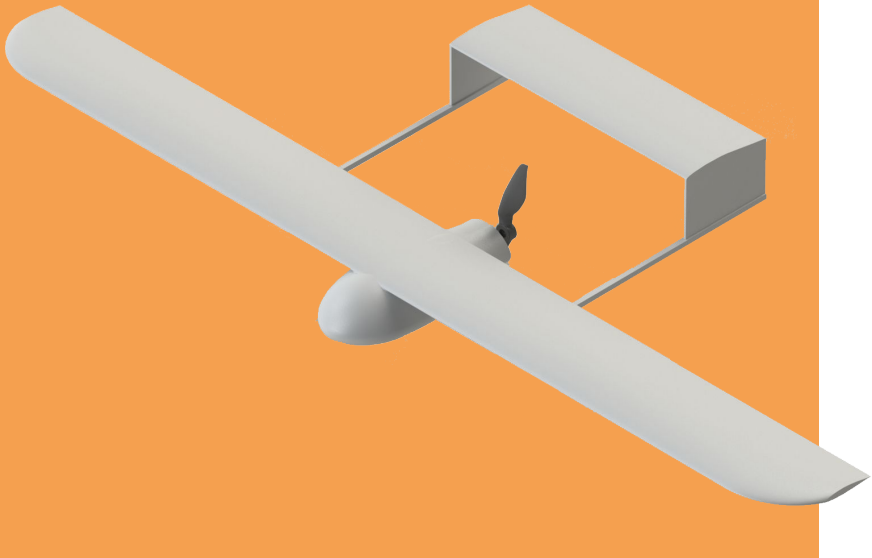


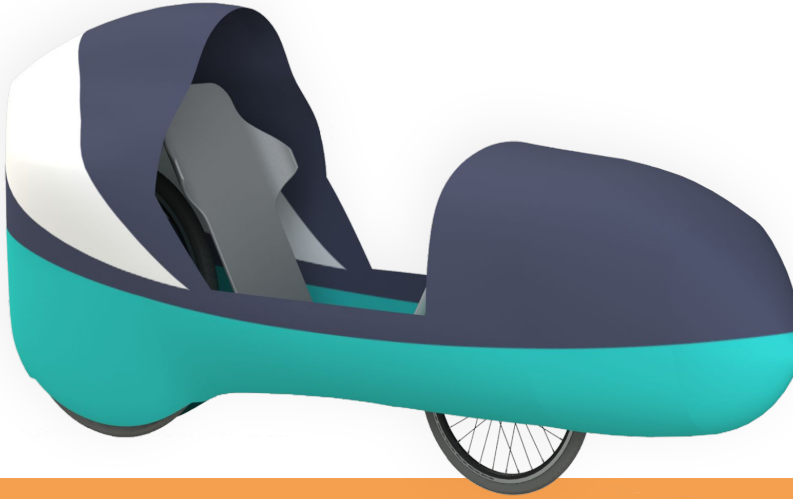
Figure: Final UAV Design

# UAV Design

Modeled the UAV design in SolidWorks and used CFD ANSYS to calculate the aerodynamic coefficients for the vehicle, checking the correlation with the expected results.

	ANSYS Results (Final Design)	Expected Results (OpenVSP)
CL ( $\alpha = 0$ )	0.42	0.4
CD ( $\alpha = 0$ )	0.95	0.02
CL ( $\alpha = 3$ )	0.75	0.7
CD ( $\alpha = 3$ )	0.12	0.027

# 02



## ■ Design and Development of a Fully Fairied Recumbent Bicycle

# Introduction

Team Raftaar, the Human Powered Vehicle Team of Delhi Technological University is focused on the design and construction of innovative, high-performance, human-powered vehicles. Team Raftaar, DTU designed, tested, and fabricated Falcon, a fully-faired lightweight, and efficient HPV to compete in ASME E-Fest Asia Pacific's Human Powered Vehicle Competition (HPVC) 2020.

The design goal was to build a vehicle with good ergonomics for rider output, excellent handling capabilities, and an advanced aerodynamic shape. The frame was designed to have a lower wheelbase and a tighter seating position to reduce the overall size of the vehicle while improving maneuverability and power output by increasing drivetrain efficiency. The vehicle configuration was selected to be a fully faired recumbent low racer configuration because of its aerodynamic capabilities.

I was involved with the team for two years, and during my time at Team Raftaar, we built two iterations of the vehicle. In 2019, I mostly learned about the concept, while in 2020, I was solely responsible for designing the vehicle frame. With the new frame design, I aimed to improve upon the shortcomings of the previous vehicle design by enhancing the riding posture for better rider comfort and optimizing the position of the chainring for better turning capabilities.

# Vehicle Design

## Ergonomics and Power Output:

- Designed for good rider ergonomics to maximize output
- Improved riding posture for better rider comfort
- Optimized position of the chainring for improved turning capabilities

## Handling and Maneuverability:

- Lower wheelbase and tighter seating position to enhance maneuverability
- Improved drivetrain efficiency to increase power output

## Aerodynamic Design:

- Fully faired recumbent low racer configuration chosen for superior aerodynamics



Figure: Vehicle Frame



Figure: Fully installed carbon fibre fairing

# Frame Design

Falcon is a low racer recumbent made from AISI 4130 Chromoly Steel. Parameter study was done according to the Whipple model, where the change in stable speed range was studied as a function of head tube angle, trail, wheelbase and front wheel diameter.

- **Front Wheel Diameter:** 0.508 m
- **Head Tube Angle:** 72°
- **Wheel Base:** 1.25 m
- **Trail:** 0.55 mm

## Drive System:

- Type: Front Wheel Drive
- Chainring: Single 60 teeth chainring
- Cassette: Shimano 8-speed cassette shifting mechanism

## Bottom Bracket and Crank:

- Bottom Bracket: Threaded
- Crank Arm Length: 165 mm

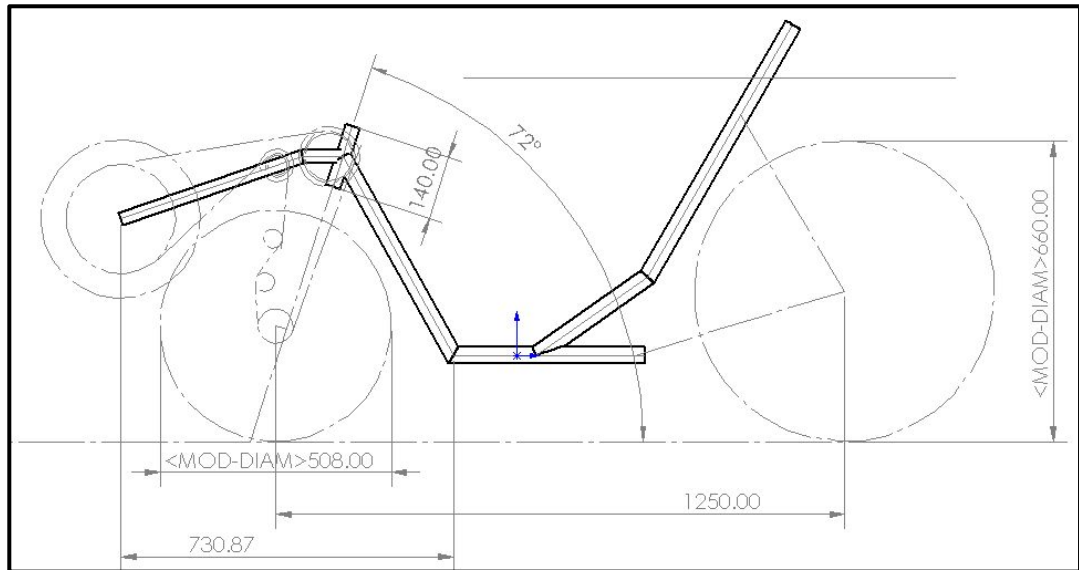


Figure: Frame Design

# Frame Design

Topology Optimization was done on Autodesk Fusion 360 by using the moment generated by a normal human being on the crank arm of the vehicle. The force values while pedaling were calculated by the use of a Force Sensitive Resistor

## Idler System:

- **Number of Idlers:** Two
- **Routing and Tension Relief:** Proper routing with tension relief for the second idler, directly routed to the derailleur
- **Weight Reduction:** Holes and/or circular patterns on the idler surface
- **Optimization:** Idler dimensions optimized to prevent chain derailment

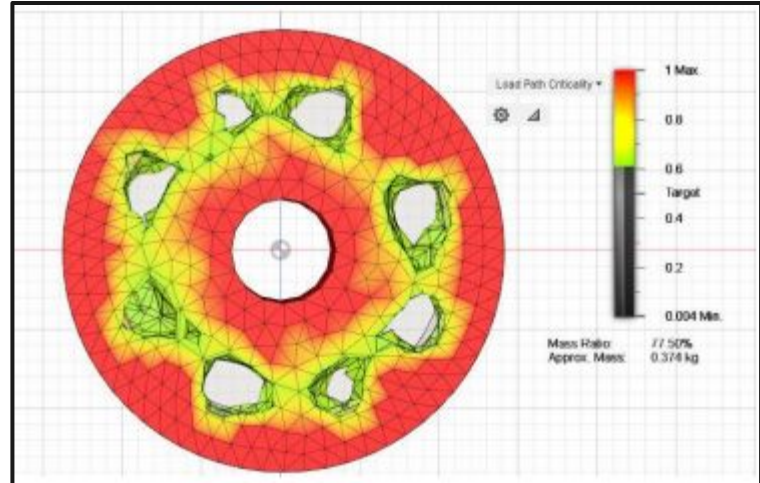


Figure: Topology Result using Fusion 360



Figure: Idlers manufactured on Centre Lathe based on the obtained result

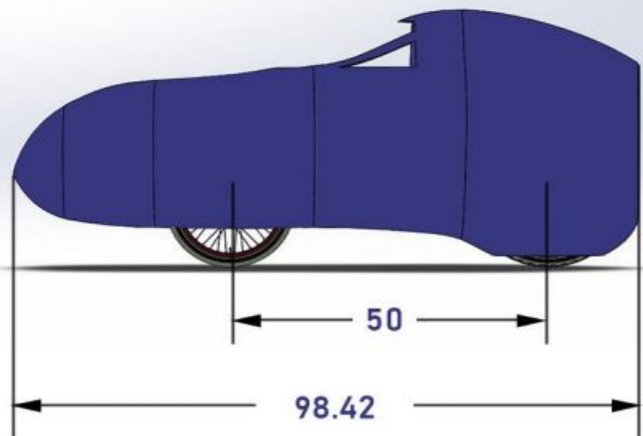
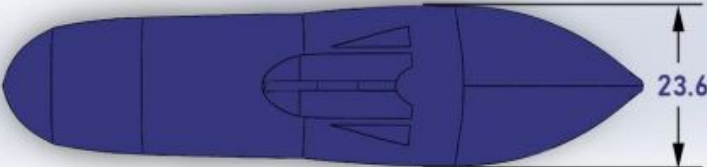
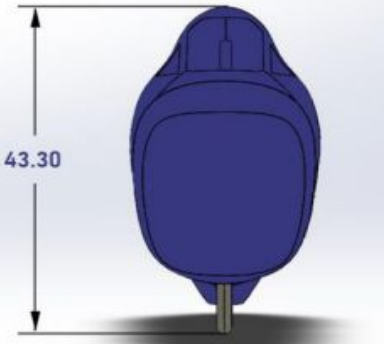


Figure: Fairing Design



# Fairing Design

## Final Fairing Shape:

- Categorized as a teardrop with a canopy
- Designed to minimize aerodynamic drag

## Design Process:

- Achieved the final design after 8 iterations
- Used a Java Applet named JavaFoil for airfoil selection
- Considered NPL ECH and NACA 6 series for the vehicle sections
- ECH 2865 section chosen for the top section of the fairing based on dimensional requirements
- Iteratively change the shape and simulate airflow using computer models

# Fairing Design Analysis

**Load Testing:** A top load and side load testing were conducted on the fairing design to ensure its structural integrity and safety.

## Top Load Testing:

- Load Applied: 2670 N
- Results: The load testing yielded a maximum elastic deformation of 0.38 cm, below ASME's 5.1 cm limit. No permanent deformation, fractures, or delamination were evident, resulting in a Factor of Safety (FOS) of 13, indicating a sturdy design meeting safety standards.

## Side Load Testing:

- Load Applied: 1330 N
- Results: The load test revealed a maximum elastic deformation of 0.193 cm, well below ASME's 3.8 cm limit. No signs of permanent deformation, fractures, or delamination were found, achieving a Factor of Safety (FOS) of 19.6, highlighting a robust design that meets safety standards effectively.

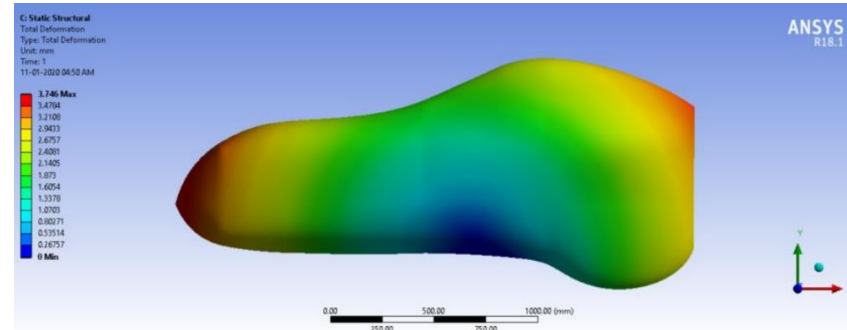


Figure: Top Load Testing Results

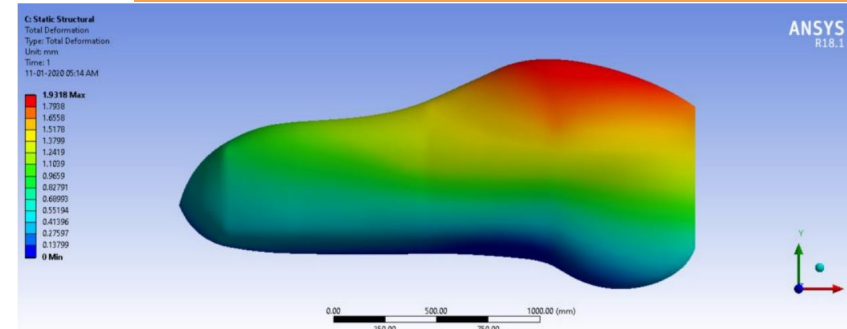


Figure: Side Load Testing Results

# Composite Layup Testing

- **Material Combination:** Four samples were made using combinations of carbon fiber and Soric Lantor as core material.
- **Surface Preparation:** Test pieces made on a plain surface coated with wax and PVA (Poly Vinyl Acetate) for easy mold release after curing.
- **Epoxy Application:** Epoxy and hardener mixed in a 4:1 ratio applied on each layer.
- **Fabrication Techniques:**
  - Hand layup technique used for the first 2 pieces.
  - Second piece covered with breather cloth and perforated film to absorb extra epoxy-hardener.
  - Both hand layup pieces vacuumed at 760 mm for curing.
  - Resin infusion technique used for the other 2 pieces, allowed to cure naturally.
  - All four test pieces cured for 24 hours, then released and visually analyzed for surface finish.



Figure: Test sample manufacturing

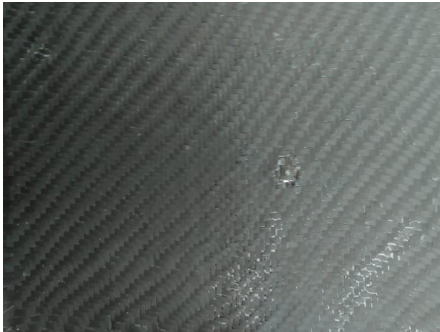
# Composite Layup Testing



Layer 1: Peel Ply  
Layer 2: Carbon Fibre  
Layer 3: Blue Foam  
Layer 4: Carbon Fibre  
Layer 5: Perforated Film  
Layer 6: Breather  
Process: Hand Layup



Layer 1: Peel Ply  
Layer 2: Carbon Fibre  
Layer 3: Soric Lantor  
Layer 4: Carbon Fibre  
Layer 5: Infusion Mesh  
Process: VARIM



Layer 1: Peel Ply  
Layer 2: Carbon Fibre  
Layer 3: Carbon Fibre  
Layer 4: Perforated Film  
Layer 5: Breather  
Process: Hand Layup



Layer 1: Peel Ply  
Layer 2: Carbon Fibre  
Layer 3: Carbon Fibre  
Process: Hand Layup

# Fairing Manufacturing

- **Design Preparation:**
  - Fairing design divided into 75 vertical parts.
  - Cross-sections of each plane printed.
- **Pattern Creation:**
  - Cross-sections cut from thermocol sheets.
  - Thermocol sheets stacked together [1]
  - Pattern sanded to achieve the required fairing shape.[2]
  - Pattern covered with a layer of glass fibre and paint to avoid any deformation and get a smooth surface finish [3]



Figure [1]: Stacked pieces of thermocol



Figure [2]: Stacked pieces of thermocol



Figure [3]: Finalized Pattern

# Fairing Manufacturing

- Pattern Division and Molding:
  - Pattern divided into 10 parts.
  - Glass fiber laid over the pattern [1]
  - Glass fiber cured to create molds.
- Mold Utilization:
  - Glass fiber molds used to produce carbon fiber pieces [2]
- Final Assembly:
  - Carbon fiber pieces seamed together to build the final fairing [3]



Figure [1]: Glass fiber curing over pattern



Figure [2]: CF Part Manufacturing



Figure [3]: All CF parts joined together to form the fairing



**Snapshots of the  
final vehicle**

# 03

## ■ Design and development of an Unmanned Aerial Cargo Vehicle

[https://doi.org/10.1007/978-981-33-4684-0\\_53](https://doi.org/10.1007/978-981-33-4684-0_53)



# Introduction



## Objective

The main objective of this study is to model and analyze the effect of the environmental conditions and design of UAVs on the load-carrying capacity of the UAVs.



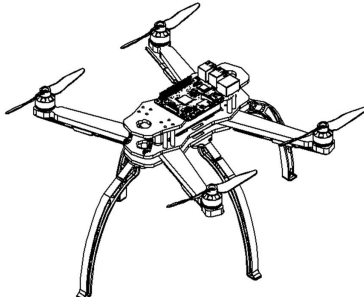
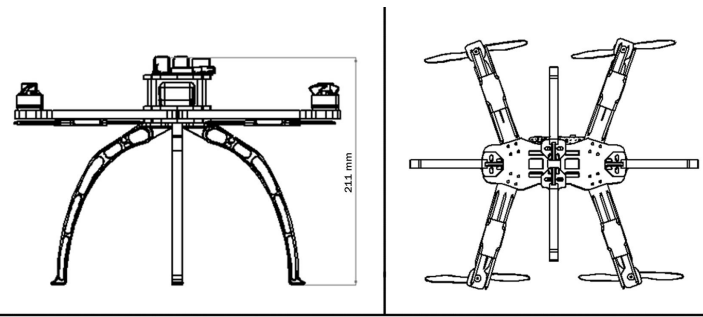
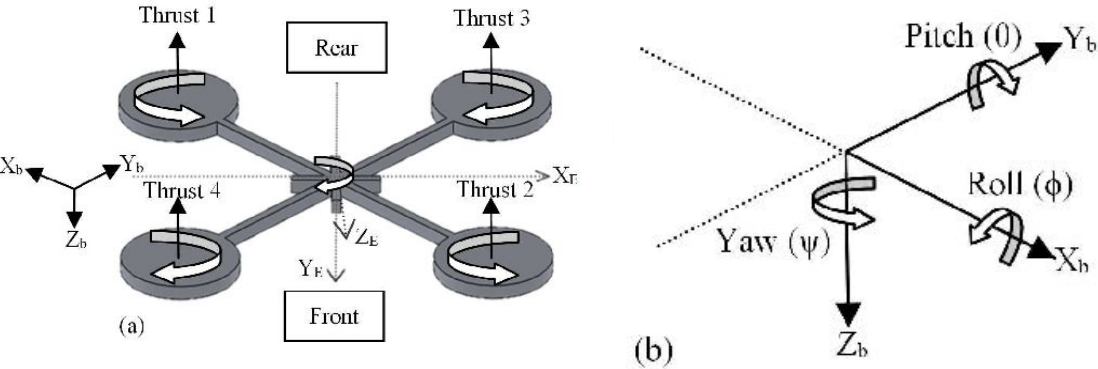
## Problem Formulation

This study helps to answer some of the questions related to a UAV such as:

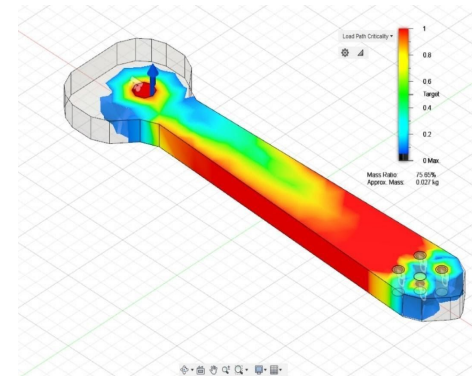
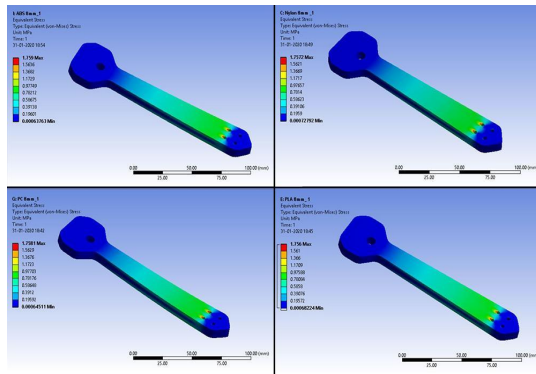
- How payload of cargo affect the other different parameters of vehicle?
- How to develop the payload carry-drop mechanism?

# Configuration

- Quadcopter layout is the most popular configuration for small-scale unmanned aerial vehicles or drones.
- Quadcopters generally have two rotors spinning clockwise (CW) and two counterclockwise (CCW).
- The Quadcopter can easily move in 6 degrees of freedom i.e. three translational directions up and down; left and right; forward and backwards and three rotational directions roll, pitch and yaw.



# Frame Arm Design



## CAD Design

- 170 mm arm length
- M3x0.5 bolt holes
- Materials : ABS, Nylon PA, PLA, PC

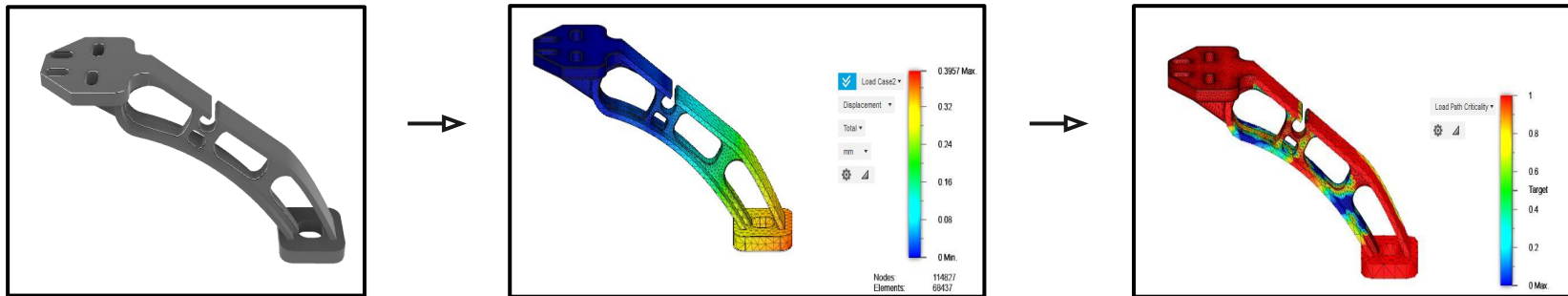
## FEA Study

- Structural Analysis
- Nylon was selected as the final material considering its machinability and low deformation.

## Topology Optimization

- Inadequate mass removal
- Determining low stress region
- Approx. 25% weight reduction

# Landing Support Design



## CAD Design

- Reduce impact forces to chassis
- Safe take-off and landing
- Materials : ABS, Nylon PA, PLA, PC

## FEA Study

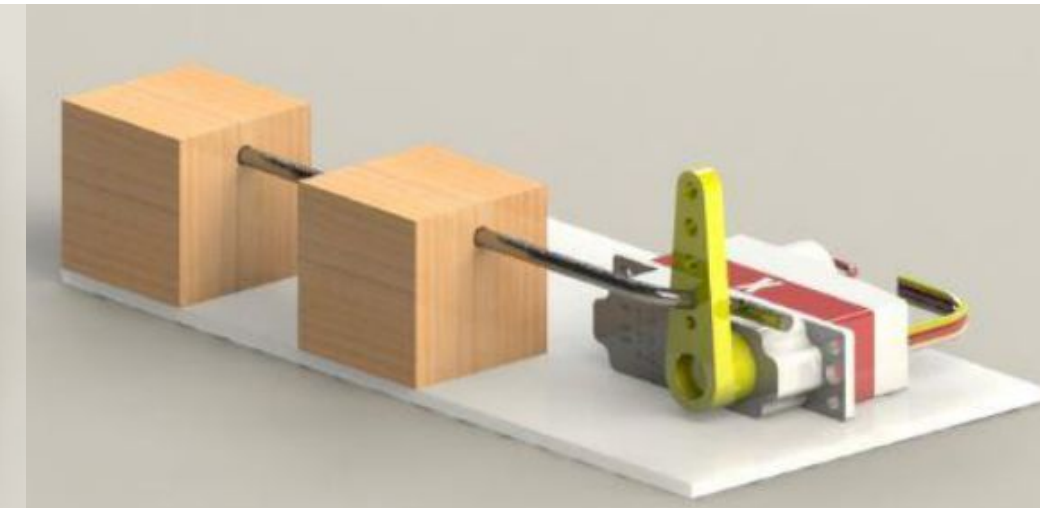
- Structural Analysis
- Nylon was selected as the final material considering its machinability and low deformation.

## Topology Optimization

- Inadequate mass removal
- Determining low stress region
- Approx. 25% weight reduction

# Pickup-Drop Mechanism

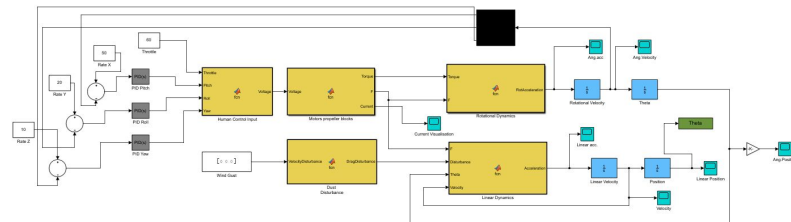
The pickup and place mechanism utilizes a servo-controlled system for precise movement, ensuring constrained sliding motion and minimal power consumption.



# Control System Design

## PID Integrated Model

- To simulate the motion of the vehicle in 3D space.
- To check the effect of different operating parameters on motion.



### Battery Performance Block

- To determine the Terminal Voltage w.r.t time

### Motor Propeller Block

- To determine the force and torque at given input voltage

### Linear Dynamics Block

- To determine the linear acceleration of the model

### Rotational Dynamics Block

- To determine the angular acceleration of the model

# Results

## Parameters Used:

- Throttle: 50%
- Rate of angular rotation:
- X-axis: 50
- Y-axis: 20
- Z-axis: 10
- Wind gust: 5 m/s in the negative Z-direction

## Conclusion:

- Design delivers excellent result to carry payload upto 350gms.
- Significant weight reduction is achieved using iterative design process.
- Faster delivery can be achieved using the UACV.

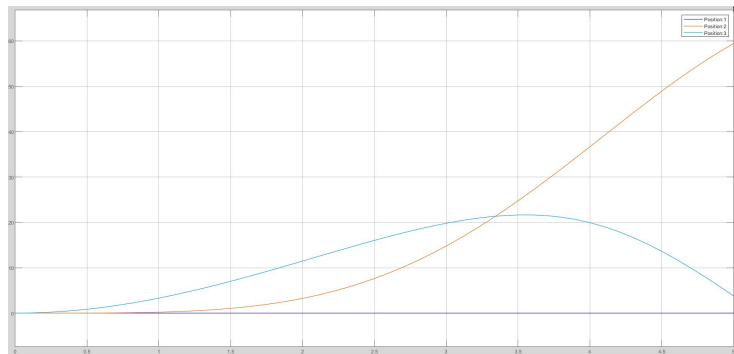


Figure: Linear position of UAV in X, Y and Z axis

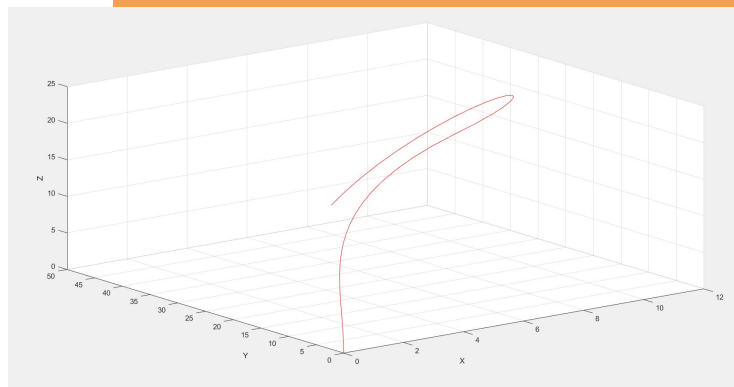


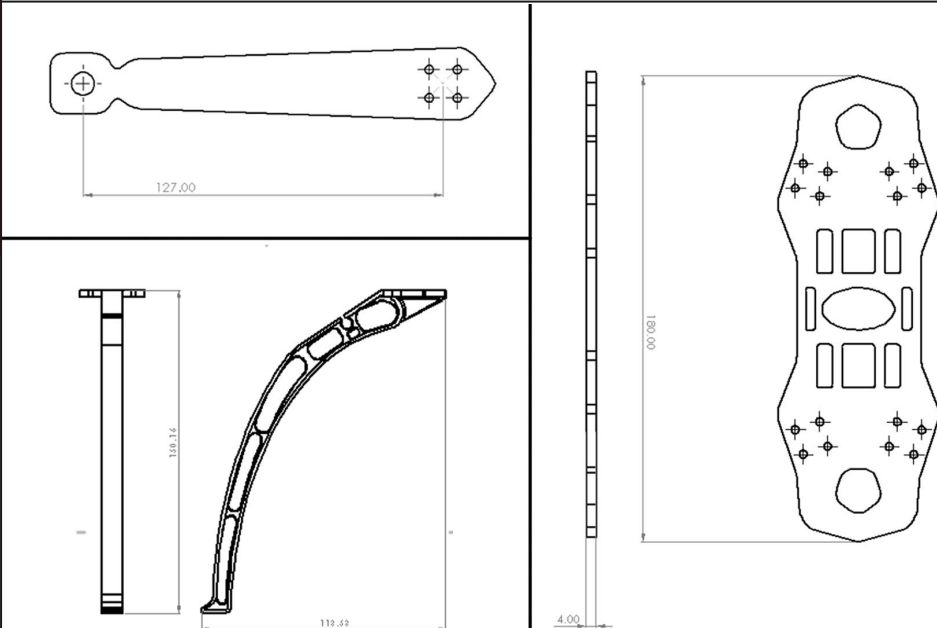
Figure: The path of UACV in 3D space

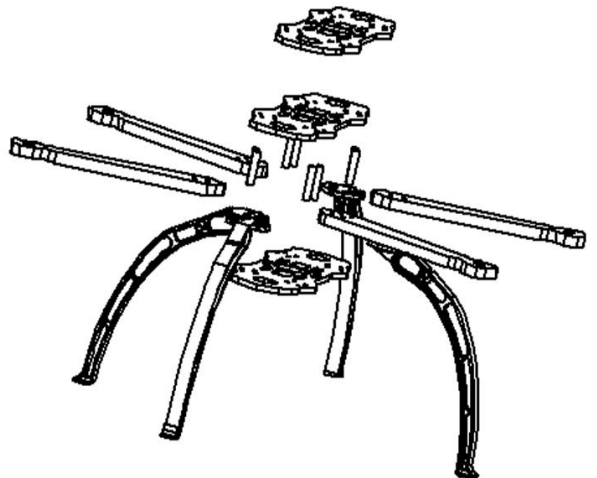
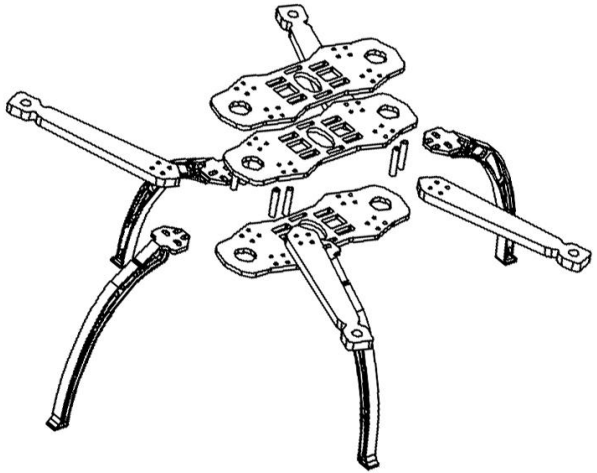


### Fused Deposition Modeling

- Nylon (PA) is used as a Manufacturing Material.
- 80% infill with 3D Honeycomb structure.

# Final Manufactured Parts





**Snapshots of  
the final vehicle**

# 04

## ■ Design and Optimization of a Mobile Robotic Arm

<https://ijari.org/assets/papers/9/2/IJARI-ME-21-06-110.pdf>



# Structural Design

## High Torque:

- When arms are fully extended horizontally, torque from the robot's weight is high.
- Stress grows closer to the rotation axis.

## Stress Concentration:

- Concentration of stress in a narrow region is undesirable.
- Heterogeneous deformation increases.

## Geometrical Change:

- Introducing a proper channel in the design can disperse loads.
- Deformation is reduced by dispersing stress to different regions.

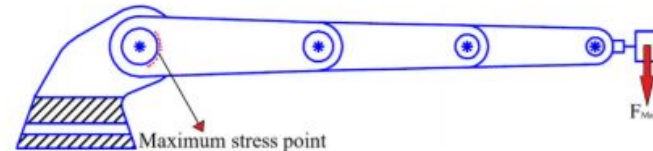


Figure-1: Illustration of fully extended articulated robot arm

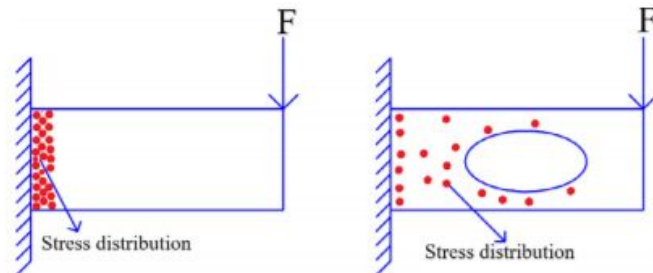
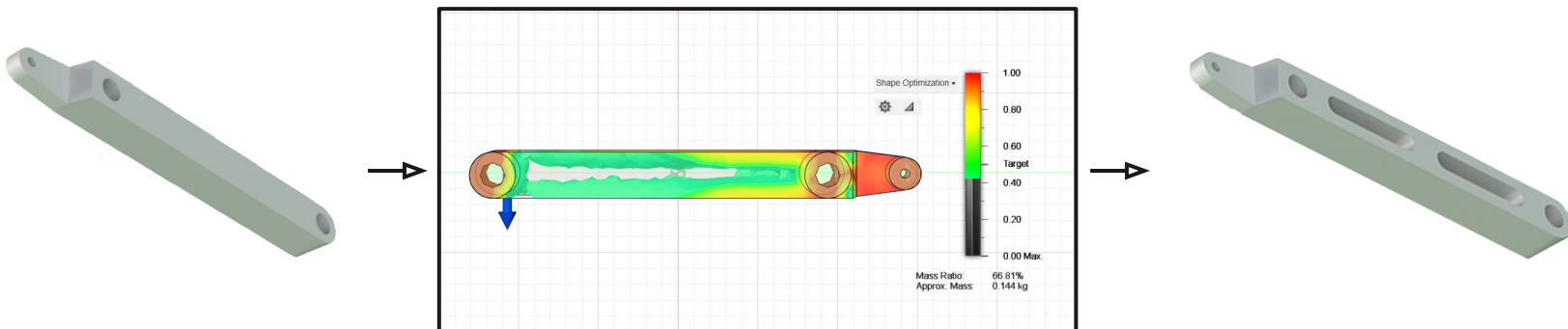


Figure-2: Diagram showing stress dispersion with geometrical changes.

# Robotic Arm Design



## CAD Design

- 250 mm arm length
- Materials : ABS

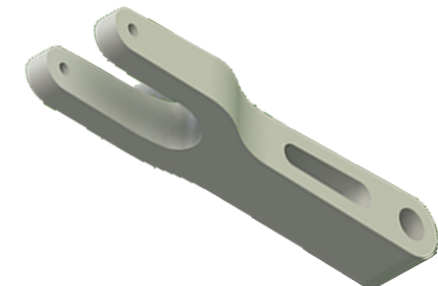
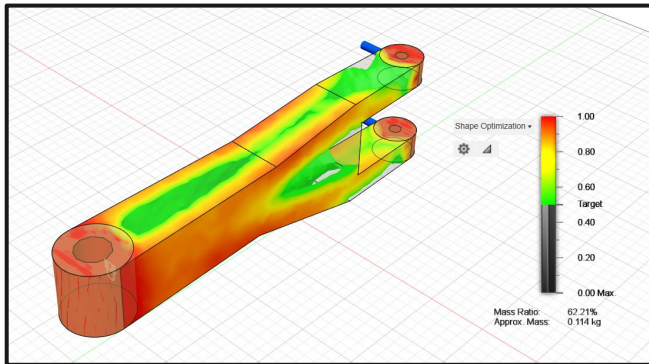
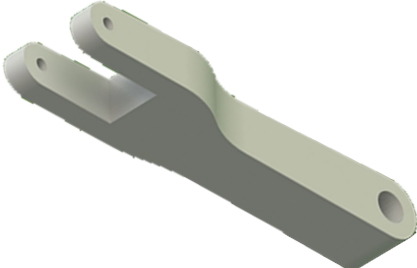
## Topology Optimization

- Inadequate mass removal
- Determining low stress region
- Approx. 25% weight reduction

## Final Design

- Designed the final arm by identifying and eliminating low-stress regions.

# Robotic Arm Design



## CAD Design

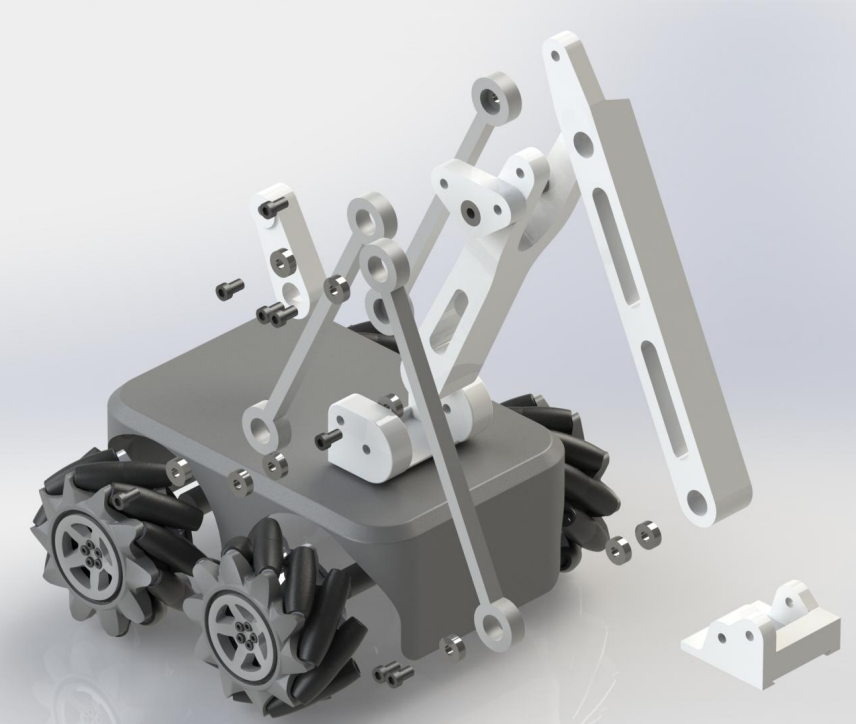
- 200 mm arm length
- Materials : ABS

## Topology Optimization

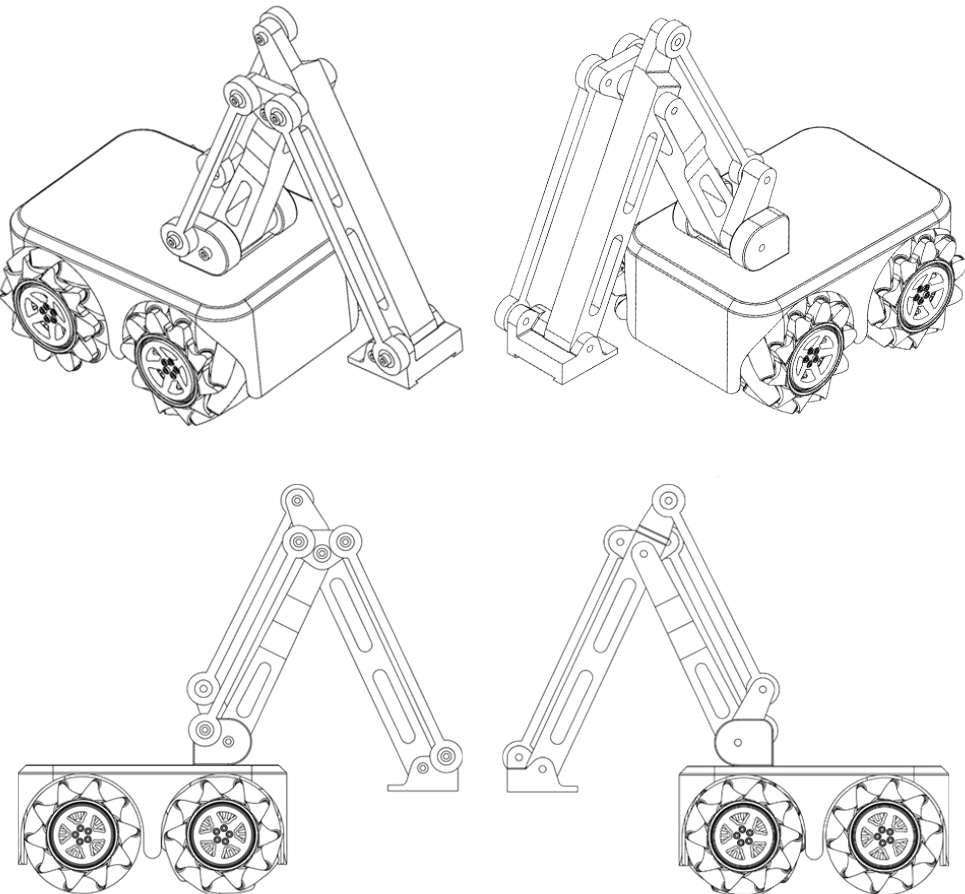
- Inadequate mass removal
- Determining low stress region
- Approx. 40% weight reduction

## Final Design

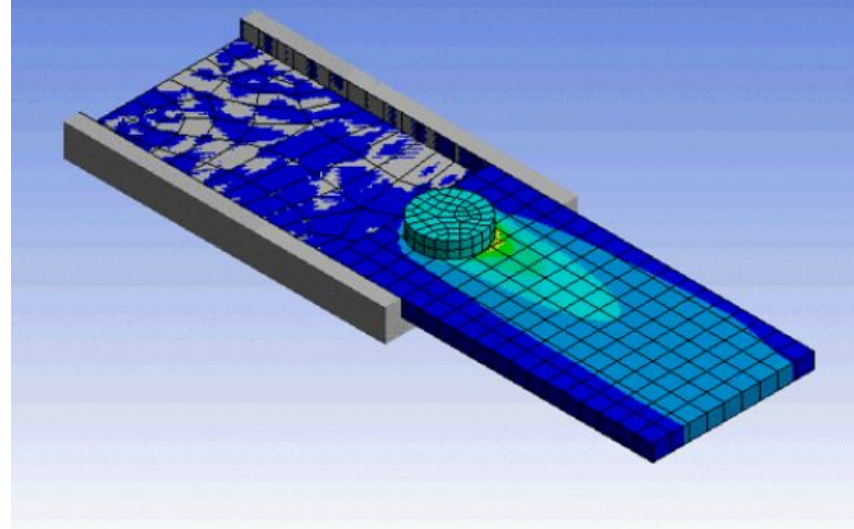
- Designed the final arm by identifying and eliminating low-stress regions.



# Snapshots of the final vehicle



# 05



## ■ Evaluating The Effect Of Process Parameters On Fsp Of Al5083 Alloy Using Ansys

<https://doi.org/10.18280/acsm.450203>

# Introduction

## Friction Stir Welding (FSW)

Friction stir welding (FSW) is a solid-state metal joining process. In this method, a non-consumable rotating tool is inserted into the abutting edges of the workpiece. The tool is then translated relative to the workpiece to form a weld along the joint line.

## Friction Stir Processing (FSP)

Friction Stir Processing is a metal processing technique based on the FSW process. FSP has found various other applications such as to increase the plasticity of materials, repair of casting defects, modification of welded joints, production of composite materials and many others

## Surface Composites

FSP is a versatile technique used for the production of surface composites. Surface composites are suitable materials for engineering applications encountering surface applications.

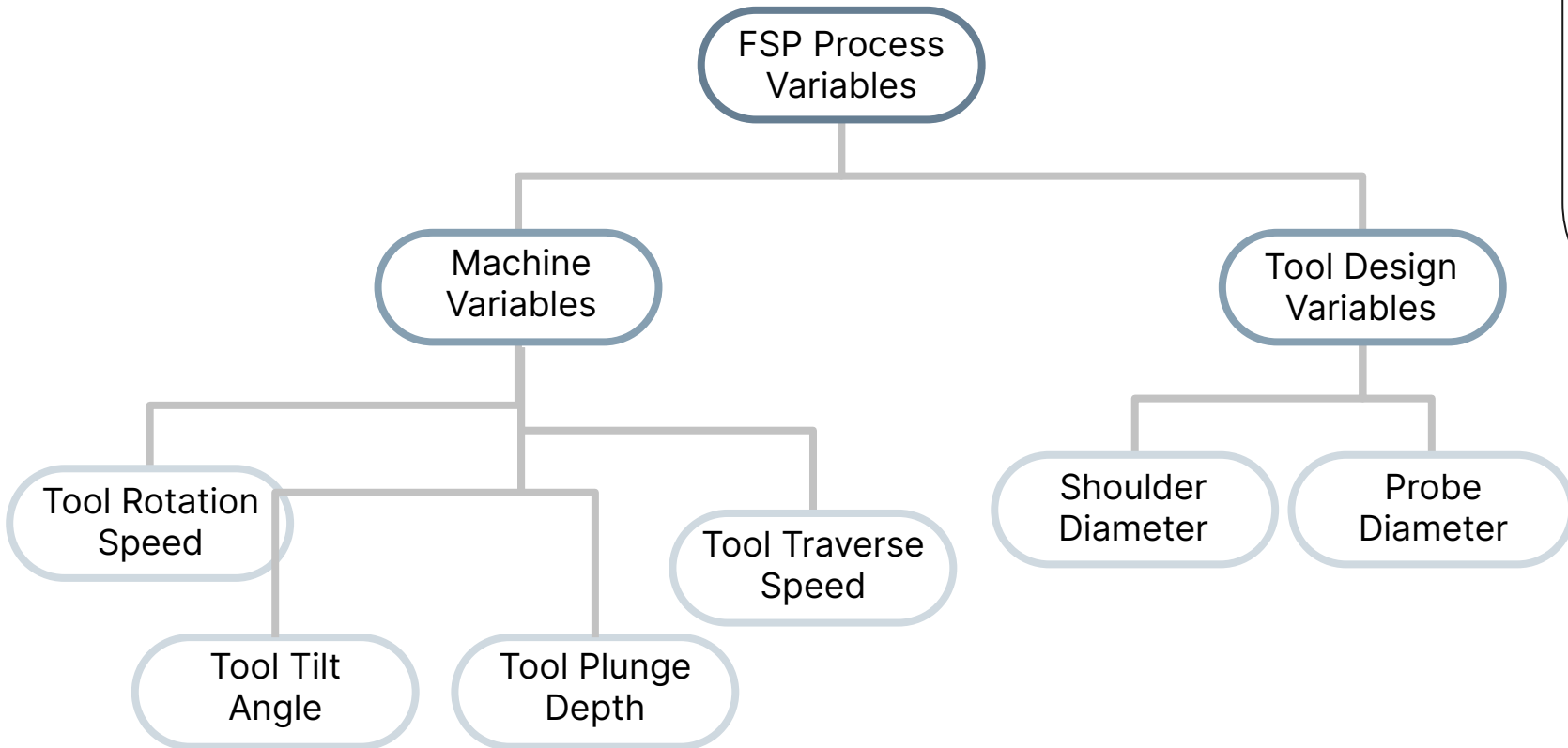
# Introduction

- Friction stir processing (FSP), compared to other solid-state processing methods, is a one-step process that attains refinement and homogeneity in its Microstructure.
- The mechanical and microstructural characteristics of the Stir-Zone can be precisely supervised by enhancing the parameters of tool design, material properties, and parameters of friction stir processing, and active heating and cooling.
- The complex configuration of various kinds of welds in FSP and their 3-D (three-dimensional) nature makes it tough to develop an overall system of ruling equations for theoretically analysing the functioning of the friction stir processed materials. The experimental trials are usually expensive and time-consuming.
- These hurdles can be overcome often by doing numerical analysis. In this study, the significance of process parameters during FSP of Aluminium 5083 and the role of numerical analysis using ANSYS Workbench in the prediction of material behaviour have been discussed.

# Research Objectives

- **Experimental Analysis:** Examined over 100+ publications on Friction Stir Processing (FSP) and documented a rigorous report on process optimization, development and applications.
- **Numerical Analysis:** A three-dimensional (3-D) thermomechanical model of the FSP of Aluminium 5083 is developed with the help of Finite Element Method using the ANSYS 18.1 software in order to understand and validate the role of process parameters in FSW.
- **Conclusion:** Four sets of process parameters were selected and a parametric analysis was conducted to ascertain the influence of speed of rotation, the translational speed, and plunge depth on the thermal field around the Aluminium 5083 alloy during the FSW process.

# Process Parameters



# Numerical Analysis

The FSP was simulated by applying the Finite Element Method using the ANSYS 18.1 software. The ANSYS software was selected on the basis of its superiority in terms of simulating mechanical properties, deformations, heat transfers and temperature distributions. The mathematical model developed for the Friction Stir Processing helps in simulating the temperature and the stress values generated in the heat affected zone.

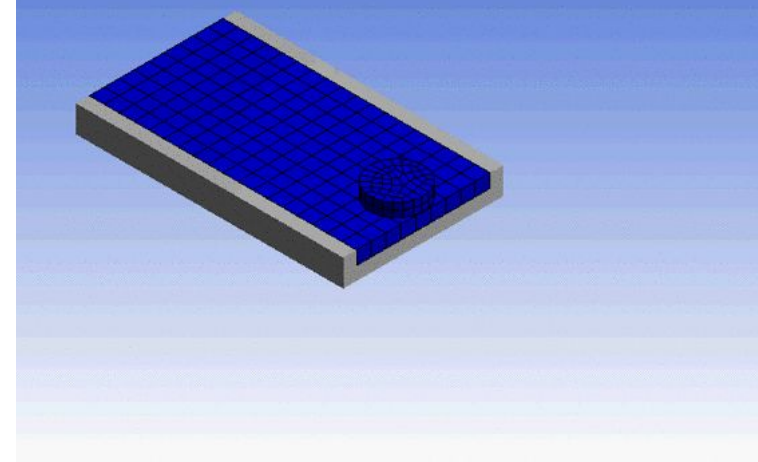


Figure: Initial Condition for analysis

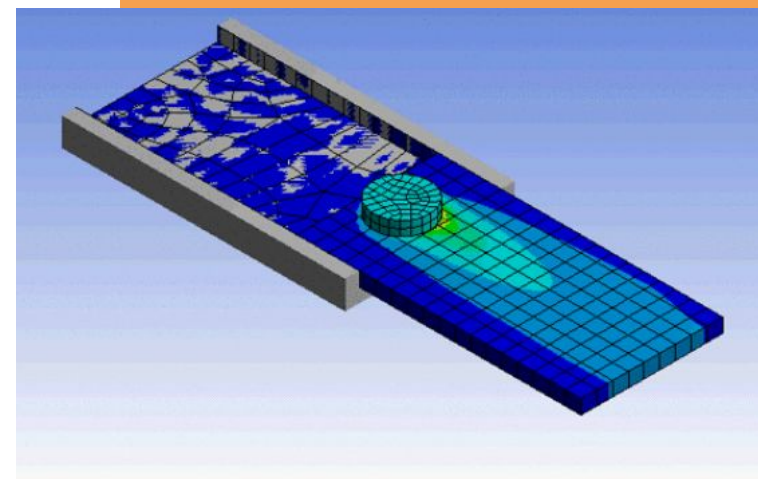


Figure: Final Condition for analysis

# Experimental Procedure

Three steps namely plunging, preheating and traversing were defined for simulation, and data was collected according to the process parameter values as presented in Table

	<b>Rotational Speed (RPM)</b>	<b>Translational Speed (mm/min)</b>	<b>Plunge Depth (mm)</b>
<b>1</b>	200	60	0.2
<b>2</b>	500	60	0.2
<b>3</b>	200	40	0.2
<b>4</b>	200	60	0.5

# Effect of Process Parameters

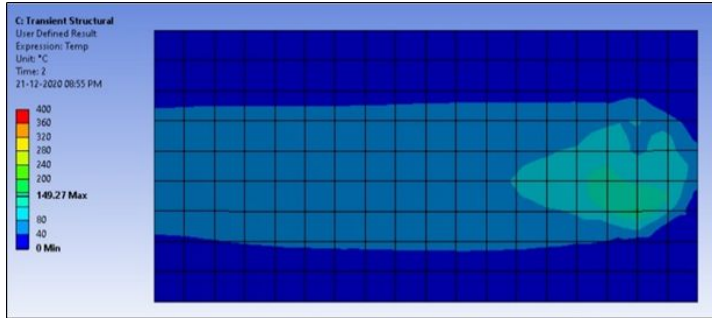


Figure Computational analysis 1 temperature results

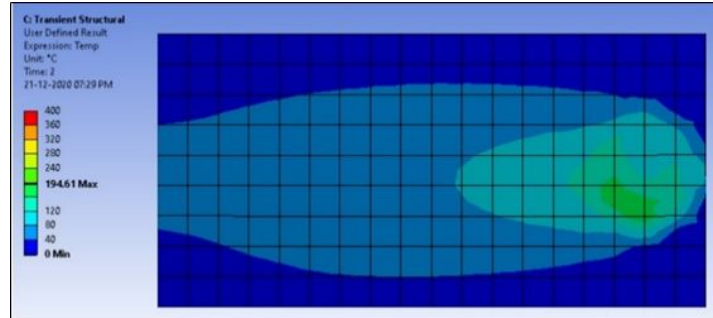


Figure Temperature results on decreasing tool traverse speed

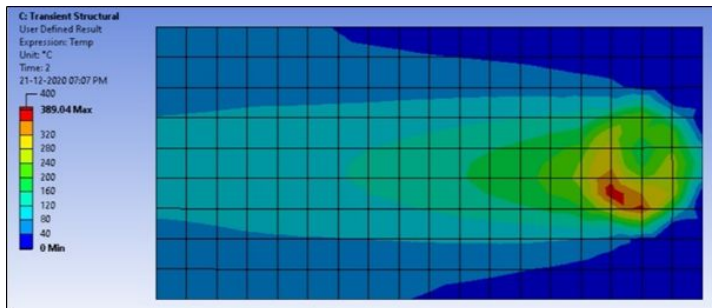


Figure Temperature results on increasing the tool rotational speed

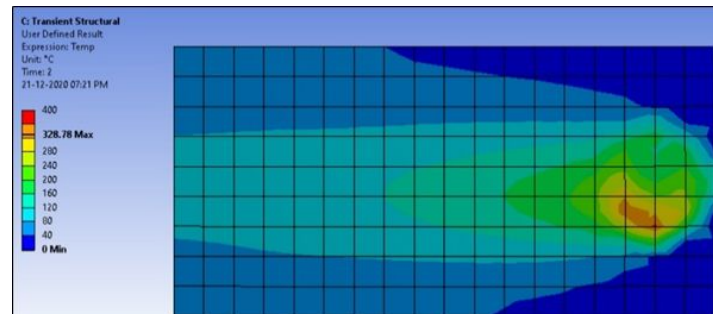


Figure Temperature results on increasing the plunge depth

# Analysis of Temperature Distribution

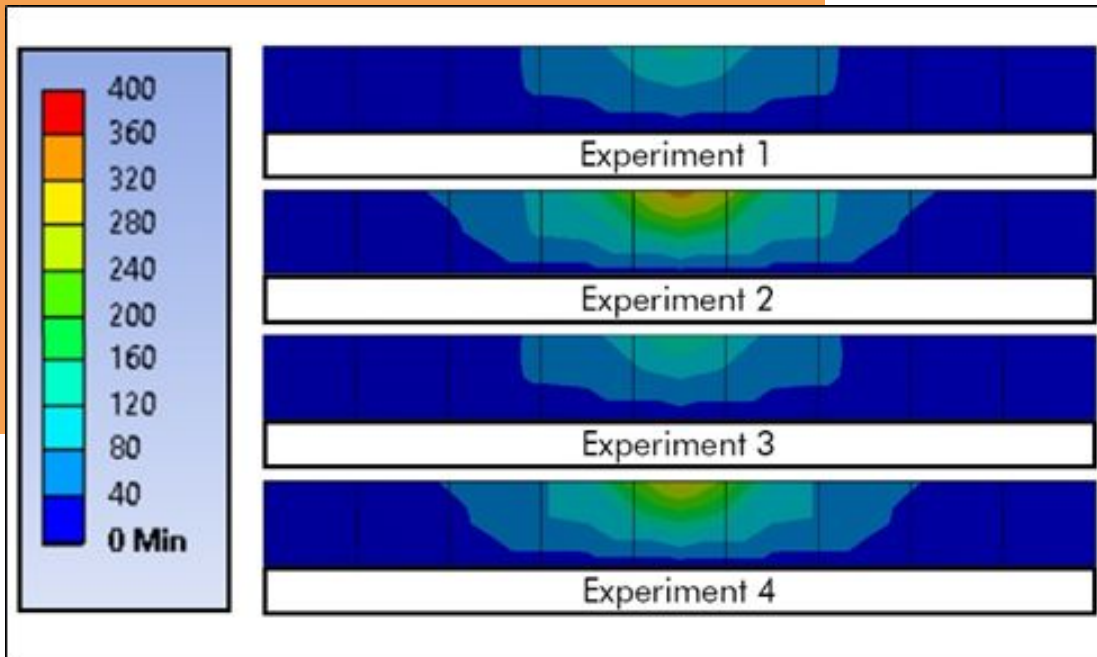


Figure: Analysis of Temperature Distribution

**Comparison of Temperature Distribution:**  
Studied along the thickness of the workpiece for four experimental analyses.

**Highest Temperature:** Observed in Experimental Analysis 2- 389.04°C.

**Heat-Affected Zone:** Increased area with higher tool rotational speed.

**Surface Distortion:** Top surface, in direct contact with the tool, is subjected to higher distortion and temperature.

**Temperature Gradient:** Temperature decreases progressively away from the tool-surface contact point.

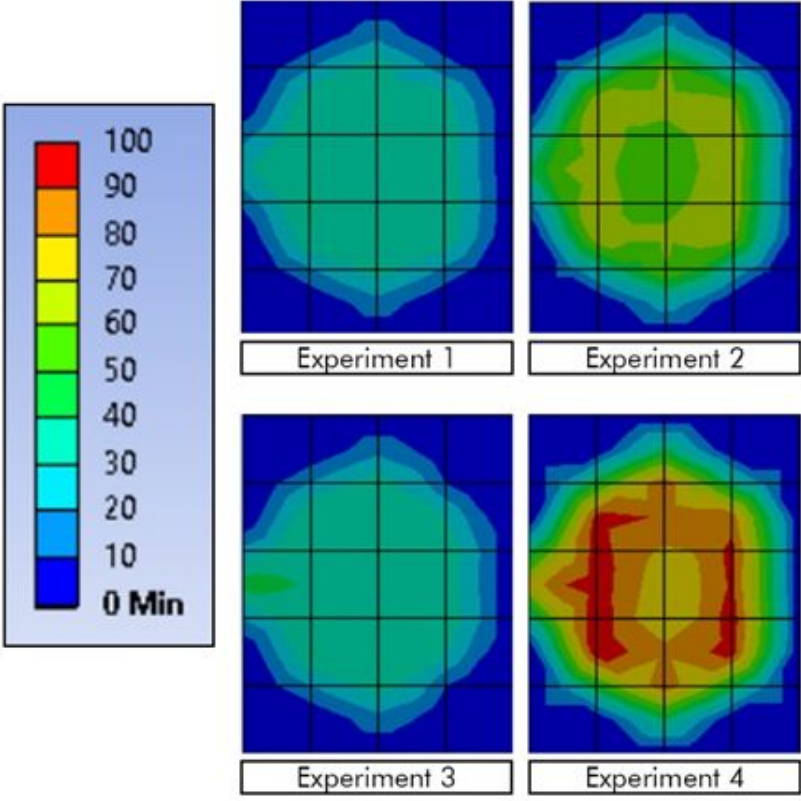


Figure: Analysis of Stress Distribution

# Analysis of Stress Distribution

## Impact of Residual Stress:

- High residual stress significantly affects post-weld mechanical properties, especially fatigue properties.
- Investigating residual stress distribution in FSW welds is practically important.

## Frictional Stress Distribution Results

- Four experimental analyses were considered.
- Highest frictional stress: Experiment 4 with higher tool plunge depth (99 MPa).

## Frictional Stress Characteristics:

- Uniform value throughout the contact surface.
- Increases proportionally to the relative velocity of the tool surface in contact with the workpiece.

# Result

- The prediction shows that the temperature is strongly influenced by the process parameters.
- The direction of tool rotation affects the temperature distribution throughout the surface to a large extent.
- The temperature increases with an increase in tool rotational speed, or a decrease in tool traverse speed.
- An increase in the plunge depth also leads to an increase in the temperature while increasing the defects in the workpiece therefore, the process parameter values should be selected carefully.
- The simulated results are expected to be helpful in optimizing the welding process to ensure good weld quality and to obtain the desired properties of the material.

# 06

## ■ Impact of Wing Sweep using Hess-Smith Panel method in Python

# Introduction

- This investigation provides valuable insights into how variations in the sweep angle influence key aerodynamic parameters, contributing to a deeper understanding of airfoil behavior and aiding in the optimization of wing design for enhanced performance.
- Conducted a comprehensive study to analyze the impact of sweep angle ( $\Lambda$ ) on the aerodynamic parameters of an airfoil.
- All parameters calculated in this study pertain to **wing sectional aerodynamic characteristics**, and can be used to calculate the overall aerodynamic performance of a wing.
- The Hess and Smith Panel Method was employed to compute the lift coefficient ( $c_l$ ), drag coefficient ( $c_d$ ), and pitching moment coefficient ( $c_m$ ) as functions of spanwise flow velocity and angle of attack.
- The boundary layer code was implemented to calculate the boundary layer thickness and the boundary layer transition point.

# Panel Method Implementation

## Analytical Method Employed

- Utilized the Panel Method to generate graphical representations of  $C_l$  vs  $\alpha$ ,  $C_d$  vs  $\alpha$ , and  $L/D$  vs  $\alpha$  for various values of lambda.

## Observations:

### 1. Lift Coefficient ( $C_l$ ) vs Angle of Attack ( $\alpha$ ):

- As the sweep angle ( $\lambda$ ) rises, the rate at which the lift coefficient ( $C_l$ ) changes with respect to the angle of attack ( $\alpha$ ) decreases.

### 2. Drag Coefficient ( $C_d$ ) vs Angle of Attack ( $\alpha$ ):

- The minimum drag coefficient ( $C_d$ ) experiences an elevation with an increase in the sweep angle.

### 3. Lift-to-Drag Ratio ( $L/D$ ) vs Angle of Attack ( $\alpha$ ):

- The lift-to-drag ratio ( $L/D$ ) attains its maximum value when the sweep angle is set to 0 (most favorable balance between lift and drag).

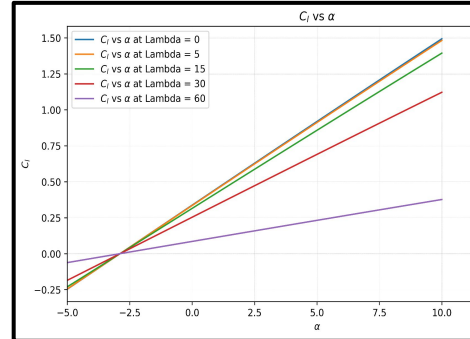


Figure:  $C_l$  vs  $\alpha$

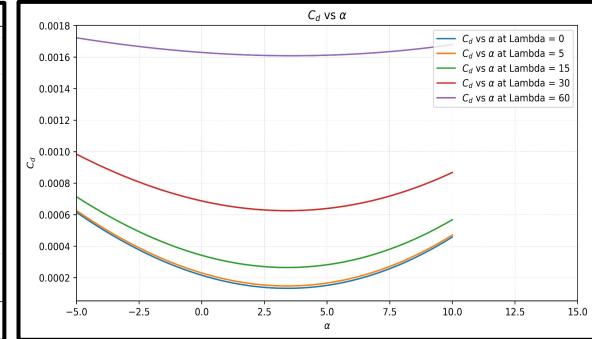


Figure:  $C_d$  vs  $\alpha$

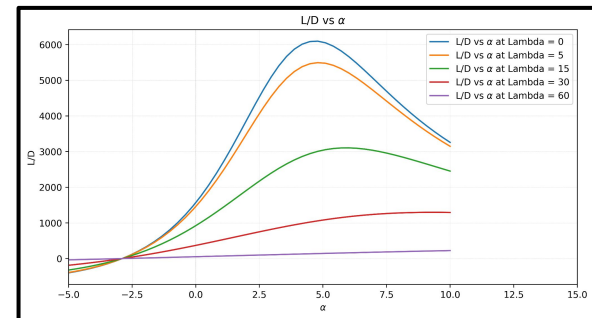


Figure:  $L/D$  vs  $\alpha$

# Impact of Sweep on Boundary Layer

- Implemented the Boundary Layer code to generate a graphical representation of boundary layer thickness for various sweep angles
- Determined the position of the boundary layer transition point using the code.

## Observations:

- One notable observation from our study is the increase in the boundary layer thickness( $\delta$ ) as the sweep angle of the aircraft wing increases.
- This phenomenon can be attributed to the corresponding reduction in the velocity of the chordwise flow.
- As the sweep angle ( $\lambda$ ) increases, it leads to a proportional reduction in chordwise velocity, indicating a direct correlation between sweep angle and boundary layer thickness.
- The position of the boundary layer transition point increases with increase in the sweep angle ( $\lambda$ ).
- This suggests that higher sweep angles contribute to delaying the transition from laminar to turbulent flow.

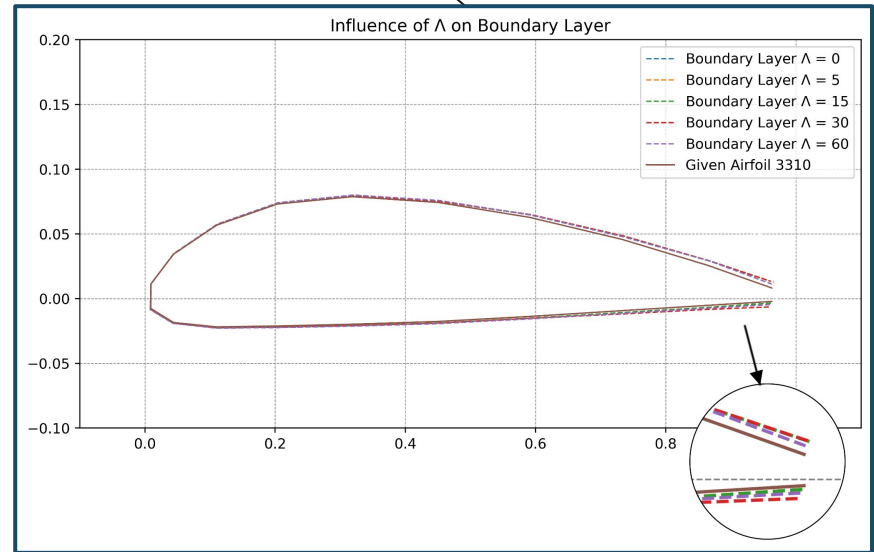


Figure: Influence of sweep angle ( $\lambda$ ) on Boundary Layer

# 07

## ■ Beam Impact Test of PVC Pipes: A Study of Quasi-Static and Dynamic Loading Responses Using Strain Gauge

# Introduction

## Objective

Examine the impact resistance of PVC pipes under quasi-static and dynamic loading using strain gauges.

## Key Findings

Disparity between expected linear elastic behavior and actual measured responses, especially under dynamic loading

## Method

PVC pipe as a simply supported beam with axial and transverse strain gauges at intervals. Loaded with weights quasi-statically and dynamically in the middle

## Implications

Insights into PVC's complex mechanical behavior, suggesting non-linear characteristics or localized material property variations.

# Detailed Experimental Configuration

**(a) Schematic Overview:** 112-inch PVC pipe as a simply supported beam with central impact force.

**(b) Strain Gauge Close-Up:** Axial and Transverse strain gauges at specific intervals.

**(c) Data Collection System:** 3-wire strain-gauge terminal boxes for strain data acquisition.

**(d) Control and Data Processing Hub:** Central control station with laptop, Ethernet Bridge, and DAQ units.

**(e) Field Setup:** Actual experimental assembly with strain gauge positions.

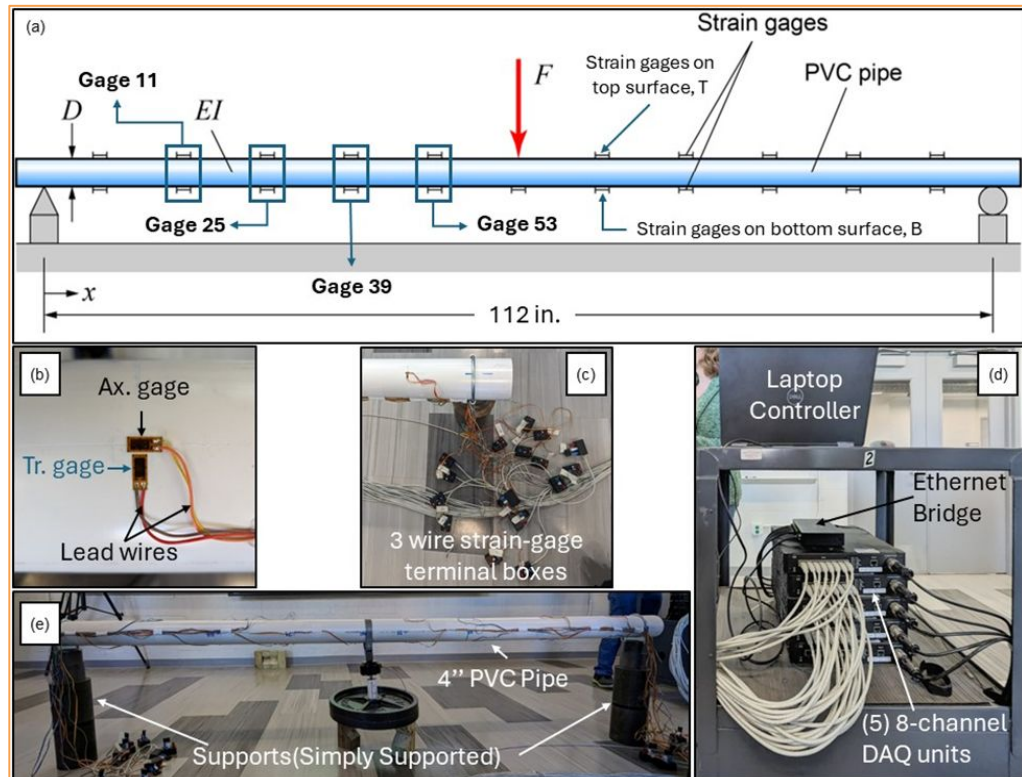


Figure: Experimental Setup

# Comparative Analysis – Quasi-Static and Dynamic Loading

1. **Applied Quasi-static Load vs Time:** Gradual increase in load over time, showing controlled load application.
2. **Applied Dynamic Load vs Time:** Sharp peaks and oscillations, reflecting sudden impact and subsequent vibrations.
3. **Strain vs. Applied Quasi-static Load:** Consistent, predictable deformation at T 11 and T 39, indicating elastic behavior under gradual loads.
4. **Strain vs. Applied Dynamic Load:** Chaotic strain patterns at T 11 and T 39, revealing complex dynamic response and significant fluctuations in transverse strains.

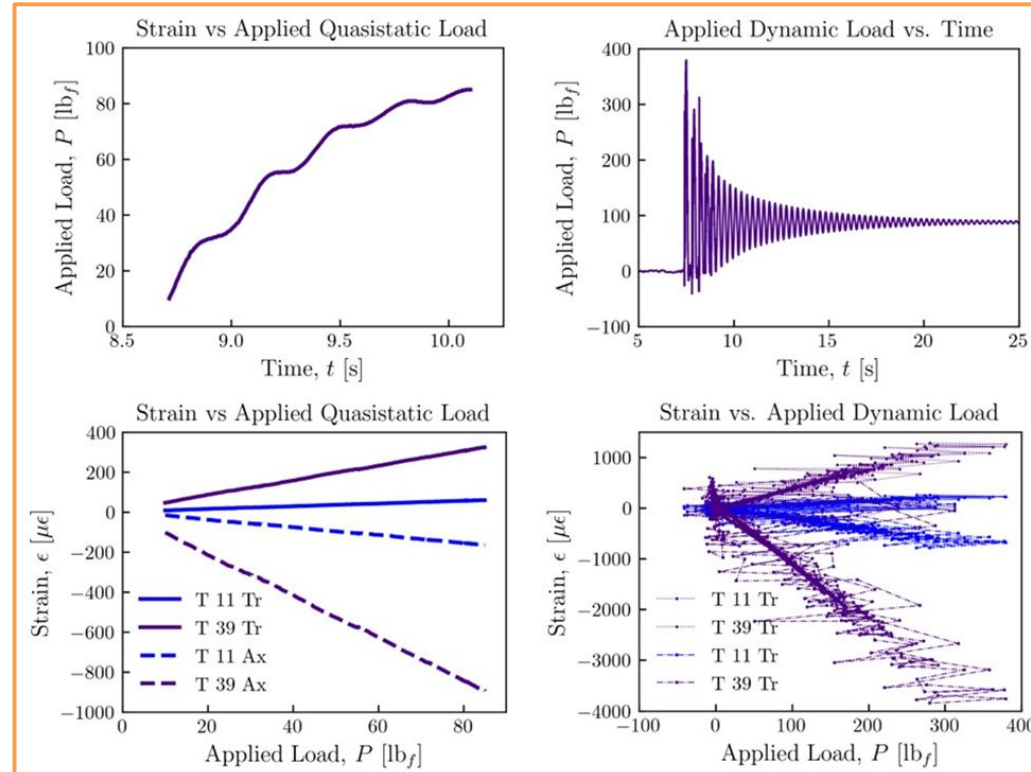
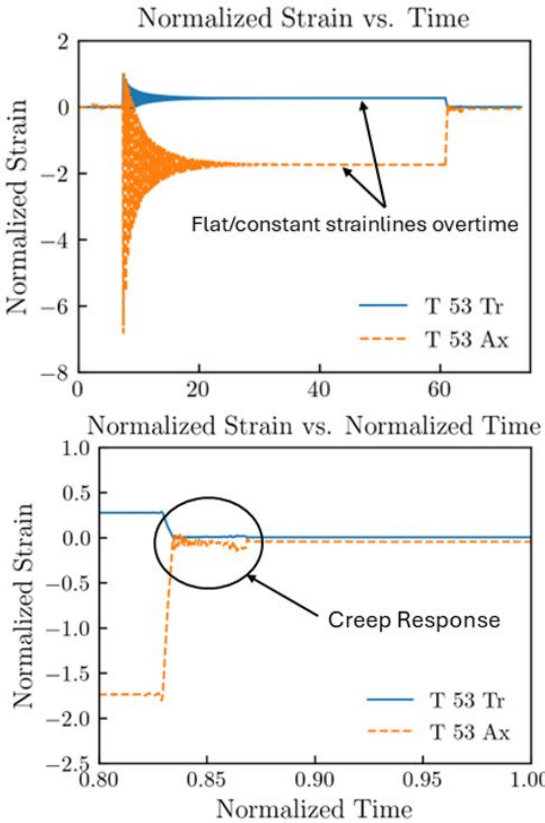


Figure: Quasi-Static Loading

# Elastic Response of PVC Pipe: Normalized Strain Analysis



- Normalized Strain Over Time at T 53:** The graph shows transverse (blue) and axial (orange) strains, with positive values indicating tension and negative values indicating compression. Post-impact, the strain lines plateau, highlighting the material's ability to endure and recover from deformation, demonstrating its elasticity.
- Creep Phase Focus:** The inset graph details normalized strain versus normalized time during the creep phase, illustrating minimal time-dependent deformation and affirming the PVC's elastic nature under constant load, with strains returning to near baseline levels post-impact.

Figure: Normalized Strain Analysis

# Static Load Strain Analysis and Fit Accuracy for PVC Pipe

## 1. Theoretical vs. Experimental Strain:

Discrepancies between experimental and theoretical strains, with T 39 showing higher strains due to increased bending moments.

## 2. Strain Discrepancies at Bottom Gauges:

Inadequate theoretical predictions highlighted by tension in bottom Ax strains vs. compression in top Ax strains.

## 3. Enhanced Numerical Fit: Improved correlation with experimental data using revised E (492.31 ksi) and v (0.36), especially at mid-span.

## 4. Consistent Numerical Fit: Uniform material behavior captured along the pipe's length, validating the numerical fit over theoretical models.

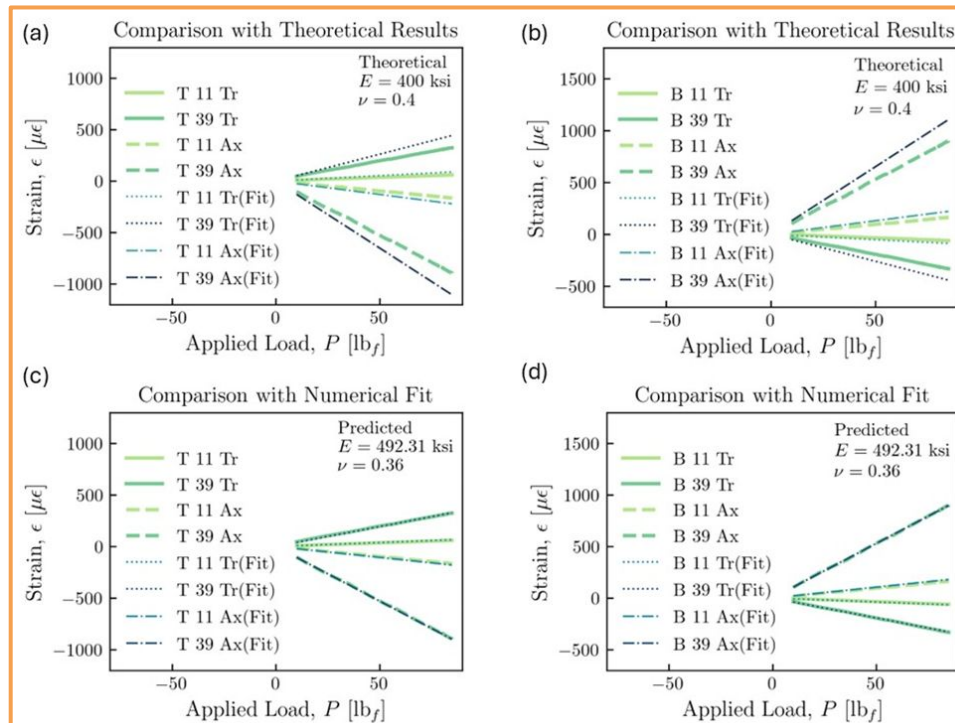


Figure: Strain load analysis

# Dynamic Strain Analysis of PVC Pipe under Impact Loading

- Strain Response at T 11 and T 39:** Experimental dynamic strain data shows initial agreement with theoretical predictions, suggesting the elastic model's qualitative adequacy in the first oscillation cycle.
- Strain at T 25 and T 53:** Initial correspondence between experimental and theoretical strains confirms the linear elastic model's applicability, with minor deviations over time.
- Strain at B 11 and B 39:** Greater strain amplitudes at B 11 and B 39 due to midspan positioning, with theoretical predictions diverging under dynamic complexities.
- Strain at B 25 and B 53:** Initial strain aligns with theoretical predictions, but the rapid diminishment post-impact highlights PVC's resilience and predominantly elastic behavior, with the linear model showing limitations under dynamic conditions.

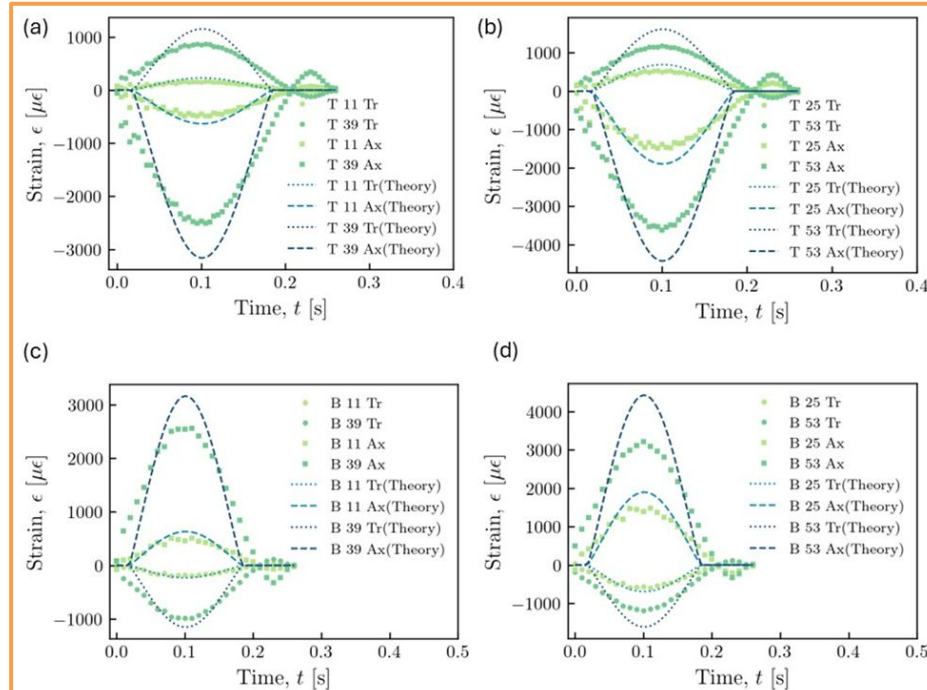


Figure: Dynamic strain analysis

# THANKS!

**Contact Details:**

ssahdev2@illinois.edu  
+1 447 902 0879



<https://www.linkedin.com/in/shouryasadahdev/>